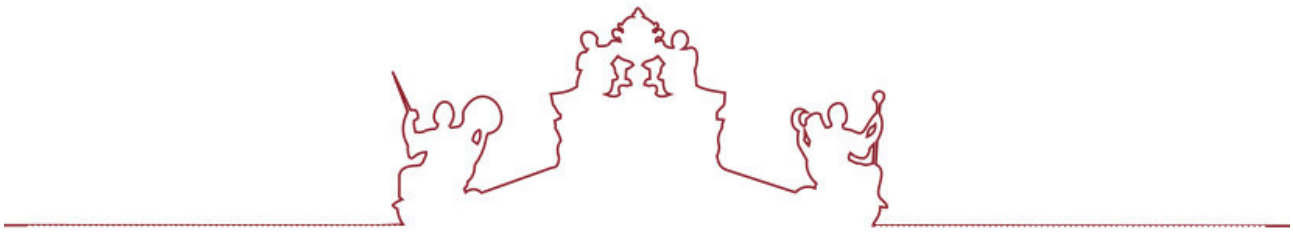

**Universidade de Évora - Instituto de Investigação e Formação Avançada**
**Università degli Studi di Roma "La Sapienza" Aristotle University of Thessaloniki**

Mestrado em Ciência dos Materiais Arqueológicos (ARCHMAT)

Dissertação

# Analysis of Chalcolithic Age lithic points from the cemetery of Torre Della Chiesaccia (Rome) (IV-III Millennium BCE): an integrated application of experimental archaeology, morphological and chemical analyses of use-residues

Leanne Thothiyil

Orientador(es) | Cristina Lemorini

Alessandro Ciccola

Évora 2023

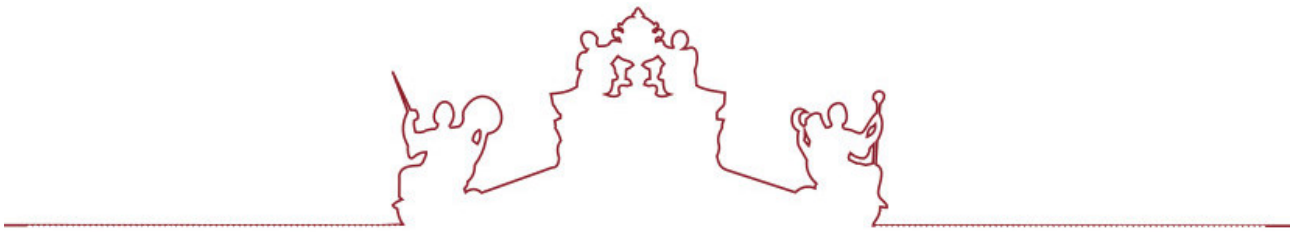

**Universidade de Évora - Instituto de Investigação e Formação Avançada**
**Università degli Studi di Roma "La Sapienza" Aristotle University of Thessaloniki**

Mestrado em Ciência dos Materiais Arqueológicos (ARCHMAT)

Dissertação

# Analysis of Chalcolithic Age lithic points from the cemetery of Torre Della Chiesaccia (Rome) (IV-III Millennium BCE): an integrated application of experimental archaeology, morphological and chemical analyses of use-residues

Leanne Thothiyil

Orientador(es) | Cristina Lemorini

Alessandro Ciccola

Évora 2023

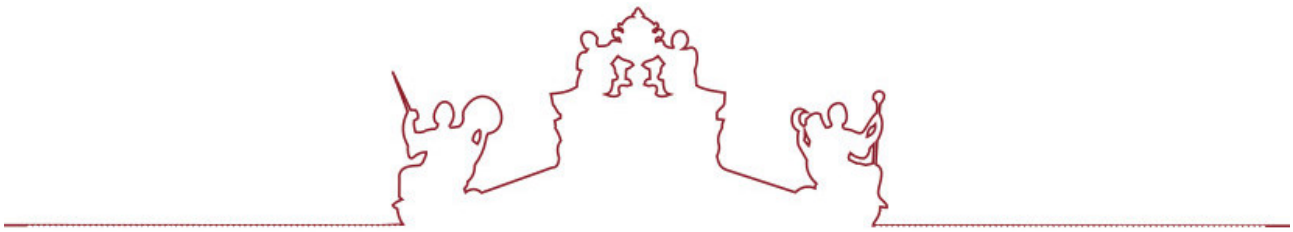

A dissertação foi objeto de apreciação e discussão pública pelo seguinte júri nomeado pelo Diretor do Instituto de Investigação e Formação Avançada:

| | | |
|---|---|---|
| Presidente | \| | Donatella Magri (Università degli Studi di Roma "La Sapienza") |
| Vogais | \| | Cristina Lemorini (Università di Roma La Sapienza)<br>Emanuela Borgia (Università degli Studi di Roma "La Sapienza")<br>Ioannis Kozaris ()<br>Nicola Schiavon (Universidade de Évora)<br>Panagiotis Spathis (Aristotle University of Thessaloniki)<br>Silvano Mignardi (Università degli Studi di Roma "La Sapienza") |

Évora 2023

# Acknowledgements

I would like to express my deepest appreciation to my supervisors, Cristina Lemorini and Alessandro Ciccola, whose constant support and constructive criticism steered me in the right direction throughout my research work.

A debt of gratitude is owed to Nicola Schiavon, Panagiotis Spathis and Donatella Magri for providing me the opportunity to pursue this master's Program.

I would like to thank Pranav Ranjan, Akash Srinivas, Andie Matulac, Kathryn Thamann, and Lionel Rumpf for reviewing my work and for their unrelenting support.

I also extend my gratitude to Sara Carraro and Rosa Crocco for their continuous support and camaraderie throughout the laboratory work.

# Abstract

Residue analysis plays an important role in determining the function of stone tools. Torre Della Chiesaccia is a Chalcolithic cemetery located in the south-eastern part of Rome, Italy and is dated to the second half of the 5$^{th}$ millennium BP. In the current study, foliate points from this site were analysed in-situ for use-residues with the help of non-destructive techniques. Digital reflected light microscopy (RLM) was used as part of the preliminary assessment for the identification and mapping of the residues on the surface of the tools. Scanning electron microscopy (SEM), in environmental mode, was applied as a second step to further characterise the morphological features of the residues and obtain clearer images. For the chemical characterisation of the artefacts, SEM coupled with an X-Ray detector (EDX) and Fourier transform infrared microscopy (FTIR-M) were used. The results of this study suggest that tools acquired from burial settings have lasting use-residues, and the combined use of instruments can be a feasible method for identification and in-situ analysis. The use of additional chemical analysis methods like FTIR-M shows that it is useful for identifying organic residues, even though some of the morphological properties of the residues aren't preserved very well.



Keywords: lithic residue analysis, chalcolithic, FTIR-M, SEM-EDX

# Contents

# List of Figures

**Figure 23:** Tool number 539224 with residue results. (a) Tool number 539224 showing residue map. (b) Brownish- whitish amorphous residues (RLM Micrograph, 200μm). (c) micro-FTIR spectrum of the residue ..... 45

# 1. Introduction

The purpose of this study is to carry out residue analysis on the foliate points that were found at the Chalcolithic site of Torre Della Chiesaccia, located in Rome, Italy. Digital reflected light microscopy (RLM), Scanning electron microscopy Coupled with an energy dispersive X-ray detector (SEM-EDX) and Fourier transform infrared microscopy (FTIR-M) were the techniques that have been used for the investigation over the course of the study.

## *1.1 Torre della Chiesaccia*

The Chalcolithic site of Torre della Chiesaccia (Figure 1), was discovered and examined as a result of preventative archaeological studies conducted in the vicinity, which were first prompted by plans for a private construction project. A collection of 13 burial chambers (Figure 2) were excavated from the archaeological site. The necropolis region is situated in close proximity to the Tor Pagnotta settlement site and is positioned roughly 340 meters to the northeast of the medieval tower known as Torre della Chiesaccia (Anzidei & Carboni, 2020a).


**Figure 1:** Map of Torre della Chiesaccia (Source: Google Earth)


**Figure 2:** Necropolis of Torre della Chiesaccia *(Anzidei & Carboni, 2020b)*

Culturally, Torre della Chiesaccia is considered to be a part of the Gaudo facies and is dated to the end of the 5th millennium BP (Anzidei & Carboni, 2020b). It is distinguished by its easily recognized features, which can be seen in the shapes of its ceramics, in the personal set of weaponry, and in the ritual fragmentation of its vases. Some of the characteristic features of this necropolis include a great number of single or double tombs containing exorbitant burial goods and some other ceremonial characteristics that are not seen in other necropolises. These features, contribute to the specific physiognomy of the Lazio aspect of these facies, making it one of a kind. It may be found across Campania and the territories that border it. It has been thought of as a component of the burial practices of nomadic or semi-nomadic groups that made use of necropolises inside of a specific area. It was once believed that the Gaudo facies was solely of a funeral type; however, further excavations in sites such as Tor Pagnotta, Casetta Mistici, Torre della Chiesaccia, and others in which grave remains appear in residential areas modified the entire picture of this culture (Anzidei, et al., 2008).

The tombs have a distinct pattern of classification, organized according to their respective locations. To the northern region lie tombs 12, 14, and 15. The central section encompasses seven tombs, with Tombs 1-5 and 7 encircling Tomb 6. The western portion comprises tombs 8 and 9. In the southwestern area, tomb 10 is situated, forming a compact

cave. Lastly, tomb 11 is integrated into an underground structure, the purpose of which remains unidentified. The tombs are characterized by their singular cell structure, with the access wells being circular or sub-circular with diameters ranging from 1.50 to 1.90 m. The surface area that is taken up by the access wells is almost never as large as the area occupied by the cells. There does not appear to be a causal connection between the dimensions of the wells and the dimensions of the cell at this time. The wells always have vertical sides, with only occasional irregularities, and the bottom is either level or slightly slanted in the direction of the cell (Anzidei & Carboni, 2020b). The entry doors of the tombs are constructed using several types of rock, including pisolite tuff, yellow tuff, basaltic lava, and occasionally tuff sourced from the "Villa Senni" formation (Anzidei & Carboni, 2020a).

While the rituals in the tombs appear to be common throughout the necropolises of the Gaudo facies, the rituals actually represent unique and complicated situations in each tomb within which they are found. The traces of rituals may be found in some of the tombs at Torre della Chiesaccia. This is proven by shards of vases that can be found at various levels of the filling in which a stratigraphic succession is not discernible, as well as from shattered vases put in front of the closing of the hypogeum. There are a few tombs (1, 6, and 7) that include artefacts that are scattered both in the well and in the filling of the cell. This suggests that there was a more sophisticated ritual that entailed the dispersal of the ritually fractured vases beyond the confines of the access well (Anzidei & Carboni, 2020b).

One of the most striking aspects of the necropolis is the particular richness of the grave goods, especially considering the small number of tombs identified. The elitist nature of the individuals buried in the necropolis is highlighted in the extensive wealth showcased by some of the goods and some aspects of the funerary ritual (Anzidei & Carboni, 2020a).

### *1.2 State of preservation*

It has been shown that the tombs' locations on the major slope of the hill are directly connected to the level of preservation they exhibit. The tombs (Tomb 8 and 9) that were situated on the highest level of the hill have suffered damage as a result of erosion and agricultural activities, and they have been preserved for only a few centimetres at most. However, the tombs that were discovered at the lowest level had a better degree of preservation than the tombs that were located at higher levels. As a result, the vaults from the tombs were preserved and were finally removed during the excavation. Even with the small quantity of data that has been obtained,

some characteristics of the hypogea may still be recognized, despite the fact that it is difficult to determine the original size of the necropolis for the reasons stated above (Anzidei & Carboni, 2020a).

Due to the poor condition of conservation of the human remains, it is extremely difficult to recognise the particular methods of depositing of the deceased within the cells for the tombs that are located in the Roman region. This is in contrast to the tombs that are located in the most extensive area of the Gaudo facies, where the inhumed have been preserved. This is because the hypogea were excavated from a particular type of volcanic rock known as "Villa Senni" tuff, which has a high acidity level. As a result, the bones completely dissolved, and only the dental crowns have been preserved. Even though the data is limited, the number of individuals and their age at death could be estimated for a few individuals; the sex couldn't be estimated for any of the individuals (Anzidei & Carboni, 2020a).

Even though it presented these challenges, the Torre della Chiesaccia Necropolis made it feasible to trace the anatomical position of the inhumed persons based on the positioning of the grave goods (Figure 3). This identification was able to be accomplished due to the fact that the cells of this necropolis very frequently include the burial of a single human (Tombs 4, 5, and 7) or two individuals (Tombs 12 and 15) with grave goods remaining in place. This allowed for the possibility of a more accurate identification of the tombs (Anzidei & Carboni, 2020b).

The present study focuses on examining the flint foliate points and knives from tombs 3, 4, 5, 7 and 14.

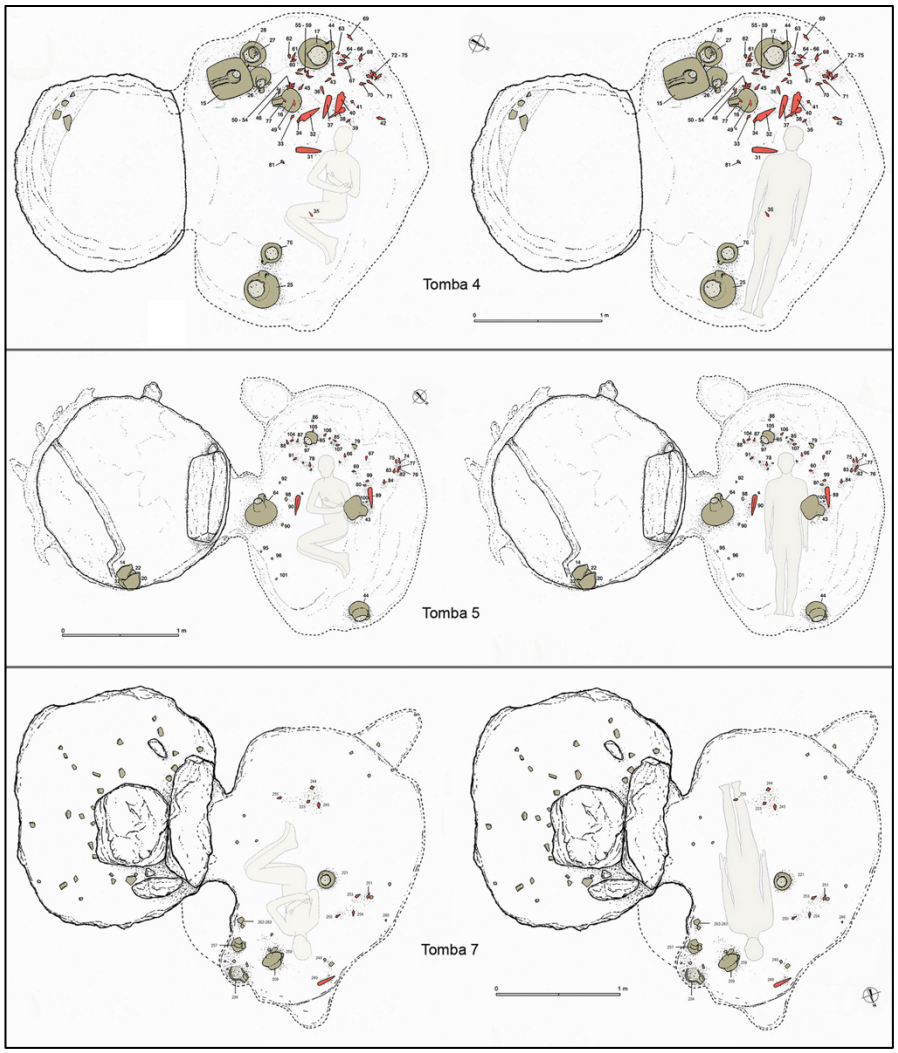


**Figure 3:** Reconstruction of the buried individuals *(Anzidei & Carboni, 2020b)*

### *1.3 Tomb 3*

Tomb 3 is an artificial grotto that has a well excavated inside of it for access (Figure 4), and its direction is northwest to southeast. It has an approximate depth of 0.50 m, a form that may be described as sub-circular, and an asymmetrical design. The major axis of the cell runs northwest to south and is roughly 2.15 m in length, while the minor axis runs east to southwest and is approximately 1.45 m in length; the height of the cell reaches a maximum of around 50 cm. Both the tomb's entry shaft and its vault have sustained significant damage as a result of agricultural operations that took place in earlier periods. The northwest corner of the room has the door to the cell, which has a narrow opening measuring around 40 cm across. As there is now no trace of any closing element, it is conceivable that the entrance to the tomb was made of a material that would have decomposed with time, such as an organic substance (Anzidei & Carboni, 2020a).

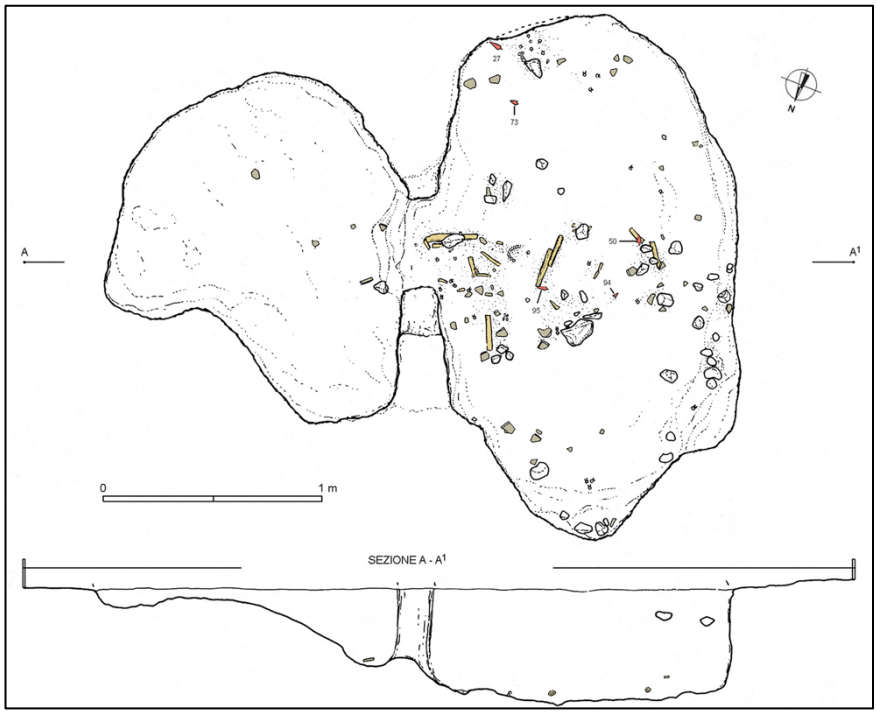


**Figure 4:** Plan and section of Tomb 3 *(Anzidei & Carboni, 2020a)*

The cell is filled with a silty-sandy soil that has a brownish-yellow hue. Only a few ceramic shards and five foliate points could be found during the excavations. All of the remains that are of an anthropological origin may be found clustered together in the middle of the room and close to the entrance. Only a few fragments of the diaphysis of long bones and a few dental crowns were found among the skeletal remains, which are in an exceedingly poor condition of preservation overall. It has been hypothesised that this structure was likely an ossuary tomb due to the fact that the skeletal bones do not appear to be those of a single individual and that the disposal of the remains is in a secondary and irregular place. These few fragments of bone allowed for the identification of two different people: one who was an adult and the other who was older than 25 years (Anzidei & Carboni, 2020a).

### *1.4 Tomb 4*

Tomb 4 is an artificial grotto that faces north-south and has an access shaft that has been cut into the tuff bank of "Villa Senni." The entrance shaft has a subcircular design with a northeast-southwest direction. The entrance walls of the tomb have sustained significant damage as a result of unlawful excavation that had taken place in the past. However, the cell was not harmed in any way by this action, and it has, for the most part, retained its integrity. The layout of the

hypogeum is semi-circular, with the major axis running northeast to southwest and the minor axis running northwest to southeast (Anzidei & Carboni, 2020a).

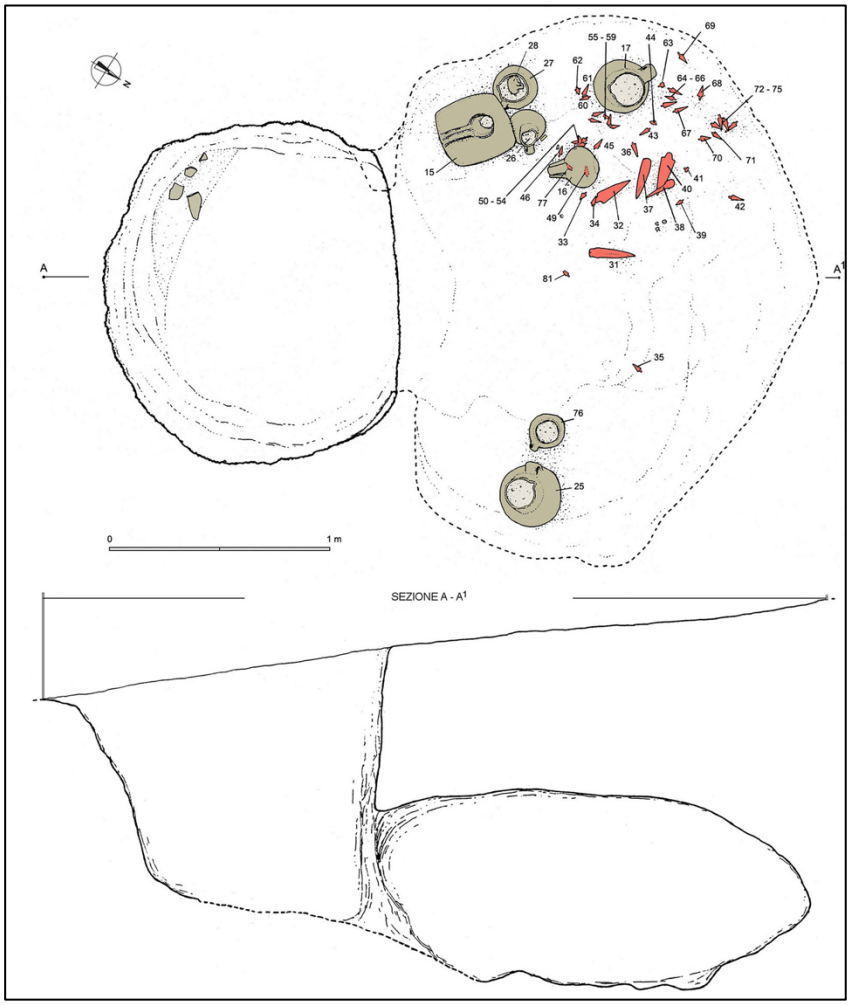


**Figure 5:** Plan and section of Tomb 4 *(Anzidei & Carboni, 2020a)*

The cell has a crumbly, homogeneous soil that exhibits a dark brown coloration, transitioning to a darker grey hue towards the lower portion of the cell as a result of the presence of a fragmented tuff layer. The skeletal remains discovered within this tomb have a restricted amount of detail, mostly consisting of a small number of teeth attributed to a single individual. The estimated age-at-death for this individual is between the range of 20 to 30 years. Based on the material properties revealed by the tomb, it is postulated that the occupant of the burial site is of an adult male. The tomb has a collection of exquisite burial items that are divided into two groups (Figure 5). The first group, which is more plentiful, is located in the western-southwestern sector, while the second group is sparser. The burial assemblage comprises a total of eight ceramic vessels, two jugs, five cups, a small number of daggers, and 41 flint foliate points that exhibit discernible signs of impact. Based on the observed spatial distribution of the

artefacts, it is possible to infer that a greater quantity of objects were positioned proximate to the head of the dead, as evidenced by the presence of teeth in that region. Additionally, it is noteworthy that the region next to Sector E is situated in close proximity to the lower extremities of the body (Anzidei & Carboni, 2020a).

### *1.5 Tomb 5*

Tomb 5 is a man-made cavern characterised by a circular access shaft that is oriented in the northwest to southwest direction. The access shaft is securely closed up by a single, solid slab constructed from piolitic tuff. The slab is shaped in a trapezoidal form and has a vertical dimension of 1.10 m. The aperture of the cell has a rectangular morphology and possesses an estimated width of 55 cm. The cellular structure has a major axis oriented in the northwest to southeast direction and a minor axis oriented in the northwest to southeast direction, with a maximum vertical extent of 95 cm (Anzidei & Carboni, 2020a).

The cell is vertically filled with sandy silt of a brown hue, interspersed with tiny to medium thickness tuff debris. Several teeth, which belonged to a juvenile human estimated to be between the ages of 7 and 10 years, were discovered at the base of the enclosure. A significant quantity of funerary artefacts (Figure 6) were excavated from the central area of the tomb, including of vessels such as jugs and cups, as well as single-edged flint daggers and a total of 20 flint foliate points. The flint foliate points are distributed in two distinct clusters, with one located in the southwestern sector of the cell, and the other comprising a smaller group positioned along the rear wall of the hypogeum. This implies the possibility that the foliate points were first preserved using a perishable substance that wasn't able to withstand over the course of time (Anzidei & Carboni, 2020a).

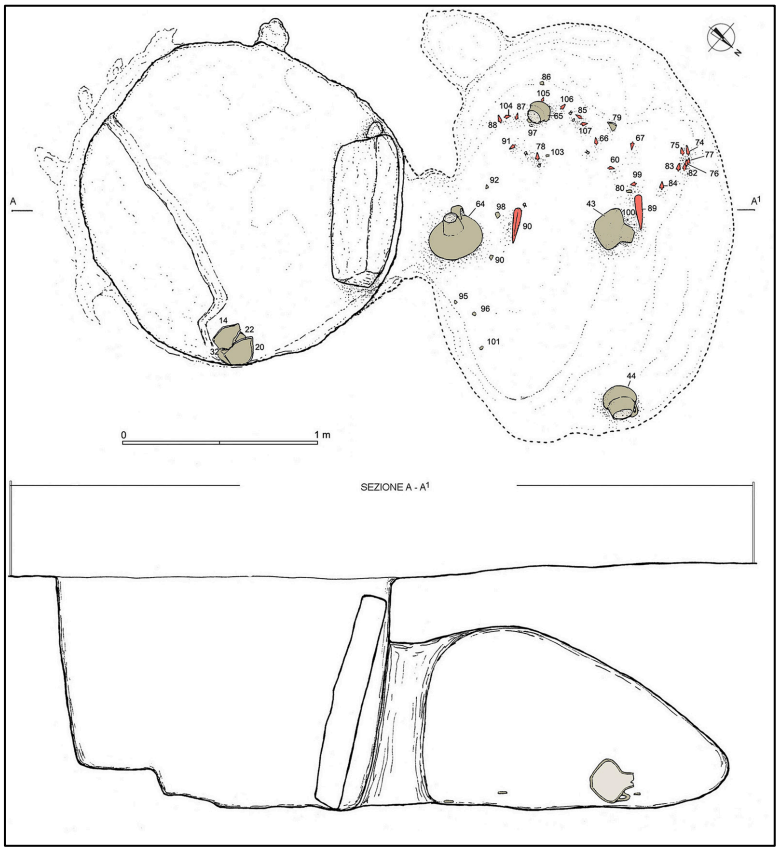


**Figure 6:** Plan and section of Tomb 5 *(Anzidei & Carboni, 2020a)*

### *1.6 Tomb 7*

Tomb 7 is a man-made tomb that is oriented in a northwest to southeast direction. The cellular structure exhibits a sub-circular morphology, characterised by a major axis oriented in the northeast to southwest direction and a minor axis oriented in the northwest to southeast direction. The vault and the well have incurred damage as a result of agricultural activities. The cellular structure has a height of 80 cm, with a gradual tapering towards the posterior region resulting in a length of 45 cm. The entrance of the hypogeum is sealed by a large, asymmetrical piece of yellow tuff, measuring roughly 1.10 m in width (Figure 7). A further segment of yellow tuff was positioned at the base of the enclosure, perhaps serving as reinforcement for the initial slab (Anzidei & Carboni, 2020a).

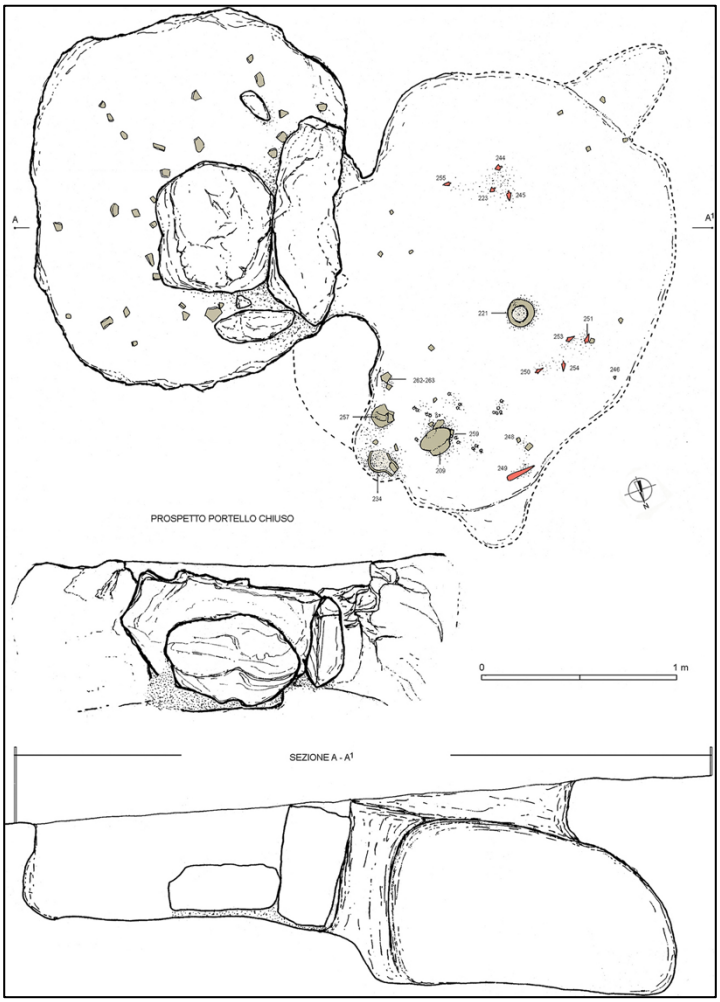


**Figure 7:** Plan and section of Tomb 7 *(Anzidei & Carboni, 2020a)*

The tomb has a uniform layer of pozzolanic soil, which is highly crumbly and originates from volcanic ash. This layer also contains a small number of pottery shards. As components of the funerary assemblage, pairs of flint foliate points were strategically positioned in the central and western regions. A collection of severely deteriorated teeth was retrieved from the eastern section of the cell, which may be attributed to a single individual aged between 18 and 25 years (Anzidei & Carboni, 2020a).

### *1.7 Tomb 14*

Tomb 14 (Figure 8) appears to represent the remaining portion of a man-made underground cave known as a hypogeum. Only the lower section of the tomb remains intact, exhibiting a northwest-southeast alignment. The cellular structure has a maximum depth of 20 cm, characterised by a major axis oriented in the northeast to southwest direction and a minor axis oriented in the northwest to southeast direction. The tomb contains a substantial quantity of fragile, yellowish-brown granular sediment (Anzidei & Carboni, 2020a).

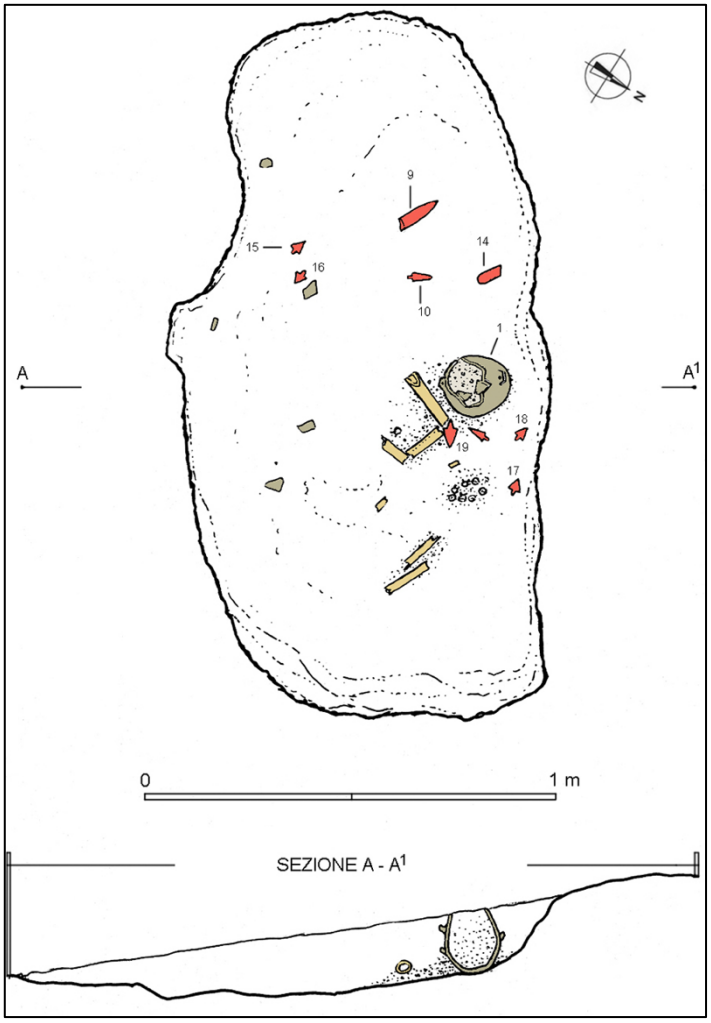


**Figure 8:** Plan and section of Tomb 14 *(Anzidei & Carboni, 2020a)*

Several skeletal pieces, such as the diaphysis of long bones and a few teeth, have been discovered in the central-eastern region. The level of preservation is quite poor, and it pertains to a solitary individual who passed away at an estimated age range of 20-30 years. The presence of overlapping diaphysis in two femurs and a tibia within the burial site suggests the possibility that this tomb might have functioned as an ossuary. The core region of the cellular structure contains several pottery fragments and additional funerary items, including jars, a flint blade, and a total of seven flint foliate points, which were discovered in two distinct clusters (Anzidei & Carboni, 2020a).

# 2. Residue analysis

## 2.1 Introduction

Stone tools are one of the few archaeological remains that have a good chance to resist the test of time and have the potential to survive millions and millions of years. For this reason, figuring out what these stone tools were used for becomes a very significant step in the process of comprehending and recreating the behaviours of ancient humans.

Residue analysis includes the identification and evaluation of preserved micro-residues, which can be either organic or inorganic, on the surfaces of stone tools. These residues may have accumulated on the surface due to the use of worked materials or as a result of manufacturing procedures (Pedergnana & Ollé, 2018) (Monnier, et al., 2013).

Stone tools are used to cut and harvest plant materials such as reeds and grasses, which results in the silicification of the tissues (Monnier, et al., 2017). When animals are butchered for their flesh and their bones are shattered for their marrow, the byproducts of this process include fat, hair, muscle proteins, and bone fragments (Monnier, et al., 2018). Stone tools are used to cut and grind the mineral source material in order to extract the valuable minerals. The use of a microscope makes it possible to see some residues, while a molecular study is required to see others. Stone tools were deliberately employed for technical or religious intentions, shown by the application of sticky glue to augment the practical effectiveness of a multi-component tool. The discovery of hafting residues (Monnier, et al., 2013) (Cârciumaru, et al., 2012) is notable since they constitute a substantial proportion of all residue findings, mostly attributed to the enduring chemical stability of lipids and hydrocarbons inside adhesive matrices. The purposeful application of pigment to implements was also seen as a means to infuse them with spiritual potency, perhaps enhancing the efficacy of hunting activities (Croft, 2021). These residues serve as significant indications of historical human activity and offer valuable insights into the lives of individuals.

The field of lithic residue analysis originated during the 1960s as a result of the contributions made by Sergei Semenov, in the study of microscopic usewear analysis. Interest in lithic usewear led to the development of residue research, with Frederick Briuer publishing the first study on prehistoric stone tool residues in 1976. The study was performed on stone tools obtained from rock-shelter and open-air locations in Arizona. These analyses involved the examination of microscopic edge wear patterns and identification of morphologically distinct plant components using conventional botanical chemical reagents. The researchers identified 37 specimens containing residues and stains from organic usage, including four from

an open-air setting. Due to complex chemicals, two samples submitted for mass spectrographic examination were unable to be identified. They were able to recognize elements but not chemical molecules (Briuer, 1976). Since then, residue analysis has been used in the detection of blood (Loy, 1983), (Nelson, et al., 1986); starch residues (Barton, et al., 1998), (Loy & Lamb, 2005), etc.

Over the years, it has developed into an effective method to determine the function of stone tools and offer insights into the use of plant and animals which otherwise would have been indiscernible in the archaeological record (Rots, et al., 2016). Residue analysis is often used alongside use-wear analysis which focuses on examining the alterations or traces on the lithic surface due to stone tool use. When combined together, it has the potential to determine the function of the stone tool independently of typological attributes (Groman-Yaroslavski, et al., 2021).

Several techniques have been employed to examine the micro-residues on lithic surfaces. There are two main methods which are employed in the analysis:

1) In-situ microscopic observations of the micro-residues preserved on the surfaces with the use of incident light microscopes. This is followed by in-situ chemical analysis of the residues for further elemental characterization.
2) Examination of extracted residues which are separated from the lithic surface with the help of a pipette or through ultrasonic cleaning (Cnuts & Rots, 2018). After preparation of the samples, these are mounted onto microscopes for observation.

### 2.2 Factors related to the cause of deposition of residues on stone tool surfaces

There are various factors which lead to the deposition of residues on the surfaces of the stone tools. This deposition of residues can take place during the life cycle of a stone tool, or even after the use and eventual burial of the tool due to various taphonomic processes. Six types of residues have been discovered using a combination of experimental research and existing scientific literature (Cnuts & Rots, 2018). These categories include manufacturing residues, hafting or prehension residues, usage residues, handling or incident residues, environmental residues, and current contamination residues.

Residues originating from production form as a result of contact with a mineral or soft hammer during the process of knapping. Hafting results in residues coming from the handle, binding, and also the adhesives; whereas prehension leads to residues related to fat and skin flakes. Incidental residues are often a result of handling of the tool and could include residues

relating to the knapper's or user's blood. Environmental contamination residues are described as those which are derived from the surrounding environment after the tool is discarded and buried because of various post-depositional processes. Site formation and diagenetic processes like bioturbation and pedogenesis can lead to residues being accumulated on the stone tool surface (Frahm, et al., 2022). Modern contaminants like skin flakes, ink, plastic, cloth fibres might result from handling during excavation, analysis, storage, etc (Cnuts & Rots, 2018).

### 2.3 Issues in Residue analysis

There are three main factors which lead to issues in residue analysis: 1. correct identification of residues; 2. the limitations of the instruments used for chemical characterisation of the residues; and 3. the disintegration of the residues due to various taphonomic processes (Monnier, et al., 2012) (Pedergnana, 2020).

One of the main issues plaguing the field of residue analysis is the correct identification of the micro-residues on the stone tool surface which have undergone extreme degradation and are often featureless and amorphous (Monnier, et al., 2018). It is often hard to discern the difference between the residue type, modern or ancient contamination and their association with the stone tools on which it was found (Pedergnana, 2020). Modern contaminants can accumulate on stone tool surface during the handling of artifacts with bare hands. This leads to the deposition of skin flakes, oils and sweat from the skin containing salt, amino acids and even proteins (Pedergnana, et al., 2016). Even though some of these potential contaminants are water-soluble and can be removed easily, some materials stick to the surface even after going through ultrasonic cleaning (Frahm, et al., 2022).

This issue is further exacerbated by the mashing of the plant and animal tissue due to stone tool use. This breaks down the structure of the tissues and makes it harder for residue identification. To combat this issue, it is imperative to be familiar with an extensive selection of experimental tissues and not just depend on histological samples. The ambiguity of the morphology of the residue is another issue. Some residues have a morphology which is discernible and can be easily assigned to their respective sources. Certain materials like hair and feather inhibit distinct morphological features which can lead to correct identification under a Visible light microscope (VLM). Despite this, a good number of residues do not possess such characteristic features and therefore, their identification becomes subjective (Monnier, et al., 2018). Fibrous materials occur in both, animal and plant tissues, and although they can be distinguishable, sometimes their features and morphologies overlap rendering their

identification uncertain. This ambiguity is also prevalent in fresh residues seen on experimental stone tools, which sparks concern regarding the residues observed on artefacts as they have undergone diagenetic processes and are therefore more prone to misinterpretation (Monnier, et al., 2012). Circumstances like trampling by humans or animals can sometimes produce abrasions among the stone tools and the bone fragments deposited together (Frahm, et al., 2022).

When the analysis is microscopy-based, the identification and the subsequent interpretation of the residues are based on the reading of the images and this is highly dependent on the quality of the microscope and the optical properties of the residue sample (Monnier, et al., 2012). The burial of the residues due to various taphonomic processes leads to a change in the morphological and colouring traits of the micro-residues and makes it even more ambiguous and hence harder to identify (Pedergnana, et al., 2016). Sometimes, the residues are also degraded into secondary products due to a variety of diagenetic processes and are shown to be replaced by fungal hyphae. Organic compounds undergo the process of oxidation or decay, whereas minerals like carbonates, phosphates and silicates go through precipitation and can also dissolve in some instances. Dissolution of bones takes place due to geochemical and hydrological activities (Frahm, et al., 2022). If the relationship between the precisely identified residues and the function/use of the stone tool are not determined properly, it might lead to the erroneous identification of the past actions carried out with the stone tool (Pedergnana, 2020).

Apart from this, the background noise caused by some of the modern contaminants while doing chemical analysis can also be problematic (Pedergnana, 2020). The application of FTIRM on in-situ residues has some challenges which may arise. In such cases, FTIRM generates reflectance spectra that may vary from typical IR absorbance spectra due to the existence of derivative and *reststrahlen* bands. The situation becomes more complicated when a residue is of such minimal thickness that the light emitted by the device is able to penetrate through it and thereafter be absorbed by the stone beneath (Monnier, et al., 2013).

The primary aim of the current research is to achieve three objectives: 1) to identify and examine the use-residues present on stone tools and describe them using both morphological and chemical methodologies, 2) to employ non-invasive techniques for conducting an in-situ analysis of the use-residues, and 3) to evaluate the feasibility of analysing residues subsequent to their washing and handling in the field. The current study aims to tackle some of the issues mentioned above by following a contamination protocol and the use of complementary techniques.

# 3. Materials and methods

## 3.1 Materials

The present investigation has been conducted employing a multi-analytical methodology. The residues were initially assessed and mapped using the Digital reflected light microscope Hirox RH-2000. The utilization of a Scanning electron microscope (SEM) was implemented as an additional measure in order to get more distinct images and conduct a more comprehensive analysis of the morphology of the residues resulting from usage. The subsequent phase of the investigation involves the chemical analysis of the use-residues which was done through the use of Fourier transform infrared microscopy in conjunction with a SEM equipped with an X-ray detector (SEM-EDX).

Before beginning the study, a reference collection was put together with the help of experimental replicas of flint tools that were acquired from the reference collection that was housed at the LTFAPA laboratory of the Sapienza University of Rome. Each of the chosen tools was put to use for an uninterrupted period of half an hour. Eleven tools in total were chosen, eight of which had their used surfaces left uncleaned after use, while the other three had their used surfaces cleaned using neutral pH soap and de-mineralized water. The foliate points made of flint that were used in the study were washed after the excavation, thus it would be helpful data to compare the distribution of residues and the state of preservation of washed and unwashed tools.

44 stone tools which were retouched in the shape of a foliate pointed tool (Lemorini, et al., 2020) were analysed for this study from different tombs from the necropolis of Torre della Cheissaccia, Rome, Italy. The tools were made from flint coming from the various formations possibly from the Latium region or from the Gargano promontory in Puglia, Italy (Carboni, et al., 2020). The flint coming from Gargano promontory documents a dense network of contacts linked to both with the North of the Peninsula and with the Adriatic side of central and southern Italy, mainly connected to medium and long-range movements and interrelationships of human groups relating to different cultural areas (Carboni, et al., 2020).

The artefacts were cleaned with neutral soap and water to remove any possible signs of environmental contamination. Demineralized water was used in the washing process. Latex gloves devoid of any powder have been used for the handling of the artifacts in order to prevent any further contamination.

The artefacts appear to be in a good state of conservation. However, the surface of the stone tools showcases slight luminosity and a glossy appearance. Due to the fact that the foliate points were buried in the tombs, mechanical abrasion seems to be highly improbable. It has been hypothesized that the acidity or alkalinity of the ground may have a significant role in the post-depositional process. Despite the fact that this did not change the lithic artifacts, it does appear to have led to the decomposition and transformation of some of the organic material that was present on the surface of the stone tools. (Lemorini, et al., 2020). The residues observed on the foliate points were embedded in sediment concretions and this probably lead to their preservation (Pedergnana, 2020). Most of the residues preserved on the stone tool surface are located in the micro-cavities and the edges containing step-fractures which results from retouches or use-edges.

## 3.2 Methods

### *3.2.1 Reflected light microscopy (RLM)*

The initial stage of the examination procedure was the identification and mapping of probable use-residues present on the surface of the stone tool. The observations were conducted with a Hirox RH-2000 Digital Microscope, with magnification levels varying from 35× to 2500×. The documentation process involved thorough recording of potential use-residues, which encompassed photographing and marking on a stone tool map (Figure 9). The residues were assigned numerical labels, such as 1, 2, 3, and so on. Subsequently, pictures with greater magnification were assigned lowercase alphabetical labels, such as a, b, c, etc. As a result, each residue may be denoted as 1a, 1b, 1c, and so forth, depending on the number of photos associated with each residue.

The digital microscope, in contrast to optical microscopes, is able to capture pictures at a greater magnification without sacrificing resolution or the need to stack images on top of each other in a different program, which may be laborious and time-consuming. This is a significant advantage over optical microscopes.

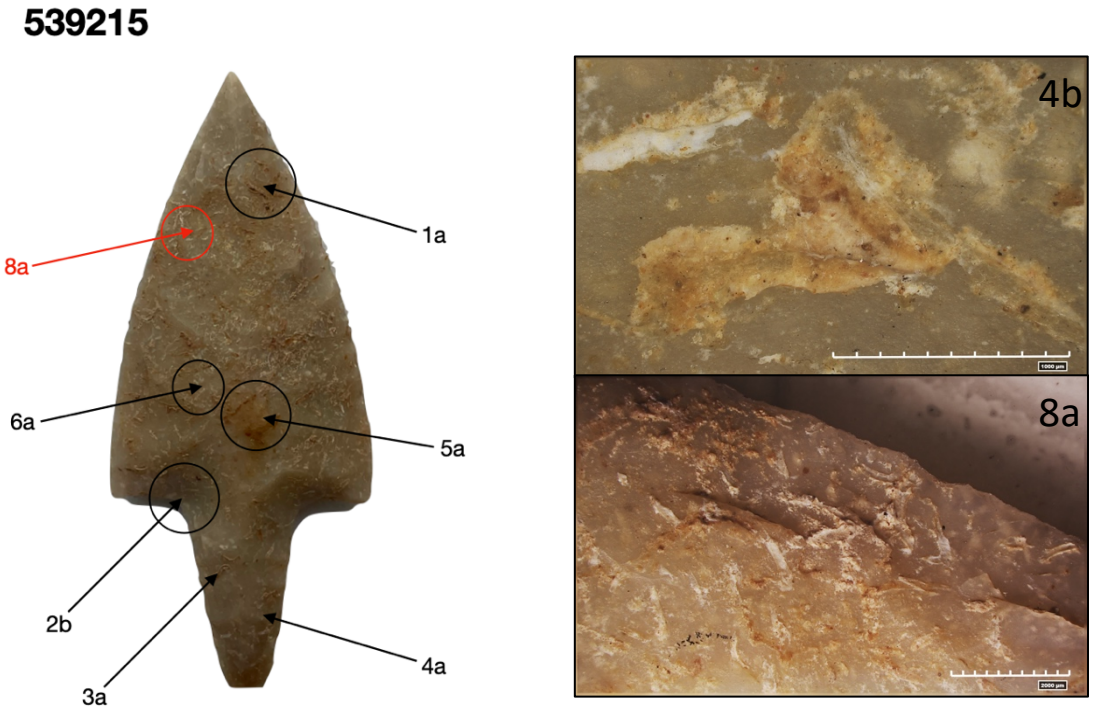


**Figure 9:** Residue map of artefact 539215. Selected RLM images of the residues, 4b (magnification 1000µm); 8a (magnification 2000µm)

In the database, only residues that contained a certain set of identifying traits like plant fibres, tissues, waxy residues, etc which are representative of use-residues were included for recording. Due to the fact that the foliate points come from a subterranean environment, the surface of the stone tool contains a number of contaminations. These contaminants were found during this initial phase and were thus omitted from the final residue database.

### *3.2.2 Scanning Electron Microscope (SEM) coupled with Energy-dispersive X-ray spectroscopy (EDX/EDS)*

After employing visible light microscopy for initial mapping and labelling, the chosen residues were subsequently subjected to analysis using a Scanning Electron Microscope (hence referred to as SEM). Given the potential time constraints associated with locating micro residues under a SEM, only the residues that were specifically selected and appropriately labelled were subjected to analysis. A Hitachi TM-3000 tabletop SEM in backscattered electron mode with an accelerating voltage ranging from 5 to 15 kV was used.

SEM has been successfully applied for residue analysis of lithics, to study adhesives employed in hafting (Dinnis, et al., 2009), (Pawlik & Thissen, 2011), (Monnier, et al., 2013), (Helwig, et al., 2014), (Wojcieszak & Wadley, 2018), (Tomasso, et al., 2020); reconstruction

of subsistence activities and tool use (Hardy, et al., 2013), (Solodenko, et al., 2015), (Zupancich, et al., 2016), (Vendetti, et al., 2019), (Lemorini, et al., 2020), (Hardy, et al., 2020), (Cnuts, et al., 2022); methodological studies (Borel, et al., 2013), (Pedergnana & Blasco, 2016), (Pedergnana, et al., 2016), (Monnier, et al., 2017), (Monnier, et al., 2018) (Pedergnana & Ollé, 2018), (Hayes & Rots, 2019), (Hayes, et al., 2019).

The SEM is a valuable tool in qualitative and quantitative research due to its ability to generate high-resolution pictures and offer visual evidence for Energy-dispersive X-ray spectroscopy (EDX/EDS) (Borel, et al., 2013). Because the samples do not need to be coated with gold or platinum while the system is in its 'environmental' mode, conducting residue analysis is made more simpler by this feature.

Numerous studies have provided evidence that the SEM is an effective tool for imaging and mapping of fragmented and tiny residues. Since organic residues have a lower atomic weight than the stone substrate, which has a larger atomic weight, the organic residue is easy to spot against the stone backdrop in SEM images. This is because the atomic weight of the stone substrate is higher. Comparatively speaking, the atomic weights of the carbon and oxygen bonds found in organic residues are smaller than those of the silica (stone substrate), which has a larger atomic weight. This distinction is represented in the SEM images, in which the lighter organic remnants seem a darker grey, which stands out against the characteristic light grey of the heavier stone substrate (Hayes, et al., 2019).

Because it is able to provide an expanded depth of field, the SEM has the potential to take micrographs with a high degree of definition. The aforementioned goal may be reached by employing an aperture that is more constricted inside the final lens, in addition to maintaining a significant working distance and employing only a moderate amount of magnification. The SEM is able to achieve a maximum image depth of 40 m at a magnification of 1000x, all while keeping a working distance of 20 mm and employing a final lens aperture of 100 m. This is possible because of the SEM's ability to maintain a working distance of 20 mm. In spite of the possible advantages that may be gained from a deeper depth of field, complications occur when the topography of the sample seems to be aligned with the residues that are already present on the stone substrate. Nevertheless, the enhanced depth of focus shows to be useful when looking at fractures and scarring in the context of the study (Borel, et al., 2013).

In the context of residue identification, colour serves as a valuable advantage. Despite the lack of colour images, SEM is capable of producing phase contrast observations when combined with back-scattered electrons. This phenomenon proves to be particularly

advantageous when residues exhibit identical colour as the underlying stone substrate (Borel, et al., 2013).

For the images to be of a high quality, the samples have to be analysed in a mode that involves a high level of vacuum. This mode needs the samples to be coated with either gold or carbon. On the other hand, when it is employed in a mode with a low vacuum, the samples do not need to be coated; nevertheless, this results in images of a poor quality. EDX analysis is used more frequently with this mode since the images do not need to be of high quality in order to be used (Borel, et al., 2013).

SEM is far more feasible when it comes to identifying residues or traces of a microscopic type, in contrast to OLM, which does not always detect residues that are extremely small in size (Borel, et al., 2013).

### *3.2.3 Fourier Transform Infrared Microscopy (FTIRM)*

In the present investigation, the infrared spectra of the residues were obtained using a Jasco FTIR410 equipped with a microscope with a 15× lens. The spectral range under observation spanned from 599 to 4500 $cm^{-1}$, with a resolution of 4 cm-1 and an accumulation of 128 scans or more. Preliminary treatment of the materials was not necessary for the analysis.

FTIR has been applied to an extensive array of research areas, ranging from the study of cells and tissues to the study of tiny molecules or chemical complexes. It is a type of vibrational spectroscopy (Monnier, et al., 2017), and it measures the vibrational energies of chemical bonds within a sample. Functional groups can be associated with distinctive infrared absorption bands that correspond to their respective vibrations. This makes it possible to study the organic compounds and minerals on a molecular level and subsequently gather quantitative results. Even though this method has several shortcomings, it offers unique insights into the characteristics of amino acids, water molecules and cofactors (Berthomieu & Hienerwadel, 2009).

Within the mid-infrared spectral range spanning from 4,000 to 1,000 $cm^{-1}$, two primary categories of vibrations are discernible. The first category encompasses stretching vibrations (ν), which pertain to alterations in bond lengths along chemical bonds. The second category encompasses bending vibrations (δ—in plane, π—out of plane), which involve variations in bond angles. The vibrational frequencies of a specific chemical group are predicted to be located within distinct regions, depending on the properties of the atoms and the chemical

bonds involved. The frequencies of chemical groups within these vibration regions are subject to fluctuation according to the specific circumstances of the group (Berthomieu & Hienerwadel, 2009).

When employed with a microscope (FTIRM), it allows the analysis of micro-residues on stone tool surfaces without having the need to extract samples (Croft, 2021). In FTIRM, the acquisition of spectral data from a limited region of the sample can be achieved by confining the illuminating area of the infrared beam through using a set of opaque apertures with predetermined dimensions. Microspectroscopic analysis of small samples is facilitated by this technique, which can be consistently employed to analyse specimens that fall within the microgram range (Bhargava, et al., 2003). Spectra can be collected using FTIR-M equipment in either the reflectance or transmission mode (Monnier, et al., 2018). When lithic residues are investigated in situ, it is only feasible to gather reflectance spectra. This is owing to the fact that transmitted light cannot normally pass through both the sample and the opaque stone that lies behind it to reach the detector (Croft, 2021).

Using the technique of reflectance (FTIRM) for the examination of residues present on stone tools is a relatively recent development. Cesaro & Lemorini, 2012 were among the first investigators to employ FTIRM as a technique for the analysis of residues. Their study focused on the characterization of residues found on obsidian and flint stone tools excavated from two Neolithic sites located in Italy. The initial step undertaken by the authors involved the generation of reflectance FTIRM spectra. These spectra were obtained from a collection of experimental stone implements that were specifically created to replicate activities from prehistoric times. Subsequently, the authors proceeded to acquire reflectance FTIRM spectra from the residues present on the artifacts. These spectra were then compared to the experimental spectra obtained in the study. The researchers were able to identify proteins, hydroxyapatite, and lipids, such as adipocere, on the stone tools by analysing the spectral peak positions.

Since then, FTIRM has been applied to several studies. A wide range of analytical techniques were employed to analyse the residues found on three stone artefacts recovered from the Palaeolithic site of Hummal, located in Syria (Monnier, et al., 2013). The microscopic remnants of residues that were subjected to gas chromatography-mass spectrometry (GC-MS) analysis previously were examined by the researchers, and their findings confirmed the presence of bitumen. The residues were thoroughly documented through the application of VLM and SEM techniques. Furthermore, the residues were chemically analysed employing

SEM-EDS, confocal Raman microscopy, and FTIRM techniques. The reflectance spectra exhibited a high level of compatibility with the absorbance typical of bitumen, as indicated by the presence of $CH_2$ functional groups at wavenumbers of 2930 and 2850 $cm^{-1}$, and the presence of peaks at 1465 and 1375 $cm^{-1}$. Nevertheless, a noticeable spectral peak ranging from 1700 to 1600 $cm^{-1}$ was observed, suggesting the presence of C=O bonds in ketones and carboxylic acids resulting from the oxidation process of bitumen (Monnier, et al., 2013).

In another study, Prinsloo, et al., 2014 chose six stone points that bear a resemblance to those commonly found in the southern African Middle Stone Age. These points were utilized in hunting and carcass processing experiments involving a blue wildebeest (*Connochaetes taurinus*) carcass. The objective was to assess the effectiveness of FTIR microscopy in identifying animal residues that had adhered to the points as a consequence of their use. Using FTIR-ATR (attenuated total reflectance) spectroscopy, they developed absorbance spectra for a variety of residue types including bone, muscle, and adipose fat. They proceeded to create reflectance FTIRM spectra for these identical residues after that. The subsequent comparisons that they carried out between these two forms of spectra indicated the presence of derivative and *reststrahlen* bands in the reflectance spectra. They were able to document characteristic bands on the FTIRM spectra of these experimental tools as a result of diverse bone, fat, and muscle residues in addition to the underlying stone since they had a reference set of reflection and absorbance spectra (Prinsloo, et al., 2014).

In 2015, Solodenko, et al., examined flint tools that were directly related with the carcasses of elephant bones which were discovered in an archaeological environment that had been well preserved at Late Acheulian Revadim, Israel. They performed use-wear and residue analysis on two flint tools, a biface and a scraper. These tools, when analysed with FTIRM, exhibit traces of adipocere, a type of animal fat, and which may be associated with activities such as butchering or working with hides. It was discovered that the scraper contained tissue and vegetable material remnants (Solodenko, et al., 2015).

Another study from the Middle Pleistocene site of Qesem Cave in Israel reveals data pertaining to the processing of animal bones, which was not done for consumption and was carried out with the use of specialized actions and specific stone tools. The identification of preserved bone residue in the form of Hydroxyapatite on the working edges of both tools was confirmed through the application of Micro-FTIR spectroscopy (Zupancich, et al., 2016).

By using an alternative methodology, (Monnier, et al., 2017) and (Monnier, et al., 2018) successfully developed the first set of reflectance infrared standards for the purpose of residue

analysis. The authors engage in a discussion regarding strategies for reducing interference originating from the stone, addressing distortions resulting from the specular reflectance of residues, and emphasizing the technique's susceptibility to differences in chemical composition. These studies include comprehensive examinations of the biochemical constituents and infrared spectra of the primary classifications of residues documented in existing literature. The materials under consideration include wood, grasses, resin, and starch grains (Monnier, et al., 2017) and muscle tissue, fat, skin, blood, hair, bone, and fish scales (Monnier, et al., 2018).

Expanding upon these two studies, another study was carried out to investigate the impact of decomposition on the chemical characteristics of various animal tissue residues, as analysed using FTIRM (Monnier & May, 2019). They accomplished this by burying stone flakes made of two different raw materials, flint and obsidian, that had macerated residues placed onto both surfaces for a whole year in a compost pile that had a damp environment. In each of the four separate trials, the breakdown of muscle proteins, keratin proteins, and hydroxyapatite follows the same pattern. The preservation of organic matter can be predicted based on the relative amounts of water and oxygen present, with microbial activity being more robust in environments containing both water and oxygen. The fact that residues are preserved better on bottom surfaces and in the deepest layers is suggestive of the fact that a lack of water and/or air slows down the activity of microbes.

More recently, (Nucara, et al., 2020) and (Lemorini, et al., 2022) have showed the importance of integrating principal component analysis (PCA) alongside FTIR for better interpretation of the results. These studies revealed that multivariate analysis of spectra can be used to differentiate between various types of tools, which include lithic tools containing protein and fat residues. PCA is a practical method for artifact recognition and classification. It does this by extracting patterns from large spectral sets and condensing the data into more easily discernible pieces, namely their most important colinear features.

# 4. Results and discussion

## 4.1 Results

### *4.1.1 Tomb 3*

1. Tool number 539108

The results of the residue preserved on Tool number 539108 from Tomb 3 is shown in Figure 10. Residue 539108_7a is located on the proximal part of the tool, preserved in the micro-fractures on the tip. The residues are brownish in colour on the edges with a waxy appearance with some tiny fibres jutting out (Fig. 10b); towards the inner edge, the residues are more whitish in colour. The micro-FTIR spectrum (Fig. 10c) shows a strong peak at 2916 $cm^{-1}$ (C–H stretching) indicating the presence of organic materials. The strong peaks between 3000 and 3800 $cm^{-1}$ attributed to the OH absorptions are due to the presence of water molecules present on the surface. Reflection spectra are used to investigate the molecular surfaces, with the intensity of the water band being attributed to the presence of water absorbed on such surface (Prinsloo, et al., 2014). The peak at 1720 $cm^{-1}$ is attributable to the carbonyl stretch (C = O stretching) and next to it are weak amide I and amide II bands (Monnier, et al., 2018). The minimum at 1048 $cm^{-1}$ is due to the interference of the stone surface.

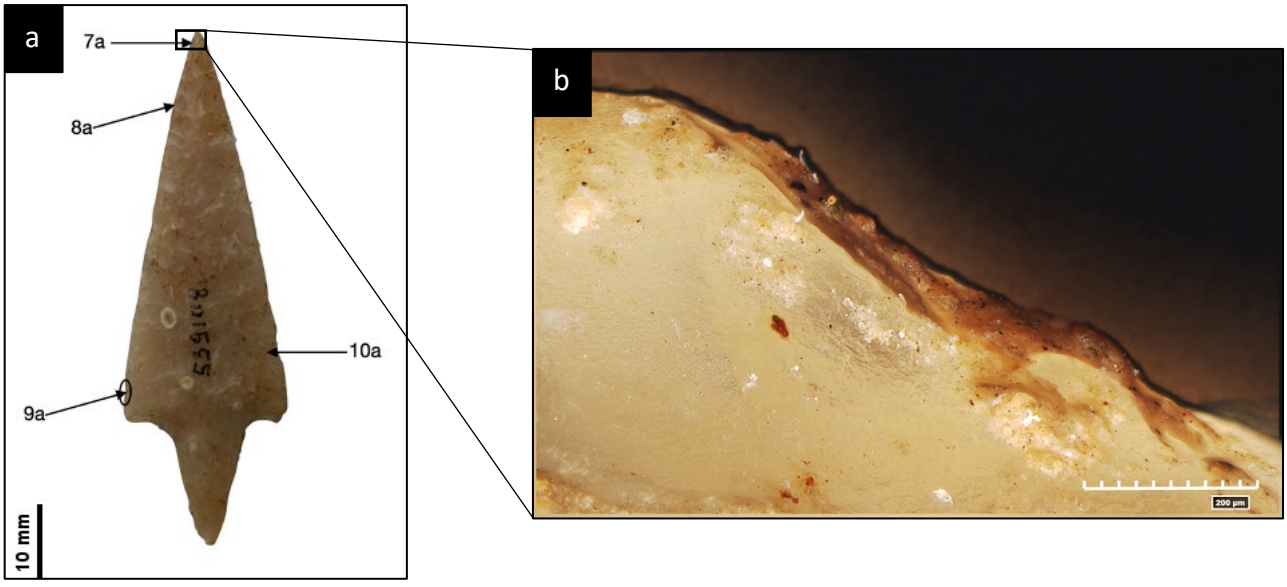


**Figure 10:** Tool number 539108 with the residue results. (a) Tool number 539108 with the residue map. (b)Brownish-whitish waxy residues (RLM Micrograph, 200µm).

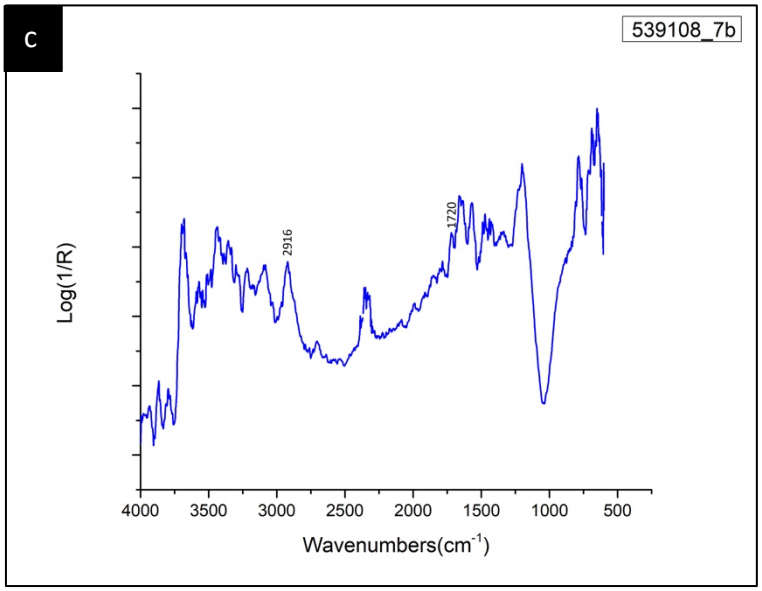

Figure 10 (c) micro-FTIR results of the residue

### *4.1.2 Tomb 4*

1. Tool number 539134

*1.1.* 539134_1a

The results of the residue preserved on Tool number 539134 from Tomb 4 is showed in Figure 11. Residue 539134_1a is located on the proximal part of the tool (Fig. 11a), preserved in the micro-fractures on the tip. The residues have a whitish, shiny and greasy appearance mixed along with sediments and red pigments (Fig. 11b). The micro-FTIR spectrum has weak peaks at 2936 $cm^{-1}$ and 2860 $cm^{-1}$ attributed to the C–H stretching which indicates the presence of organic materials. The peaks at 1720 $cm^{-1}$ (C = O stretch) and 1537 $cm^{-1}$ ($CH_x$ bending) (Monnier, et al., 2018) again indicate the presence of organic materials present on the stone tool surface. It is hard to characterise exactly the kind of organic material as the peaks appear different due to degradation of the material and contamination due to sediments (Hayes & Rots, 2019).

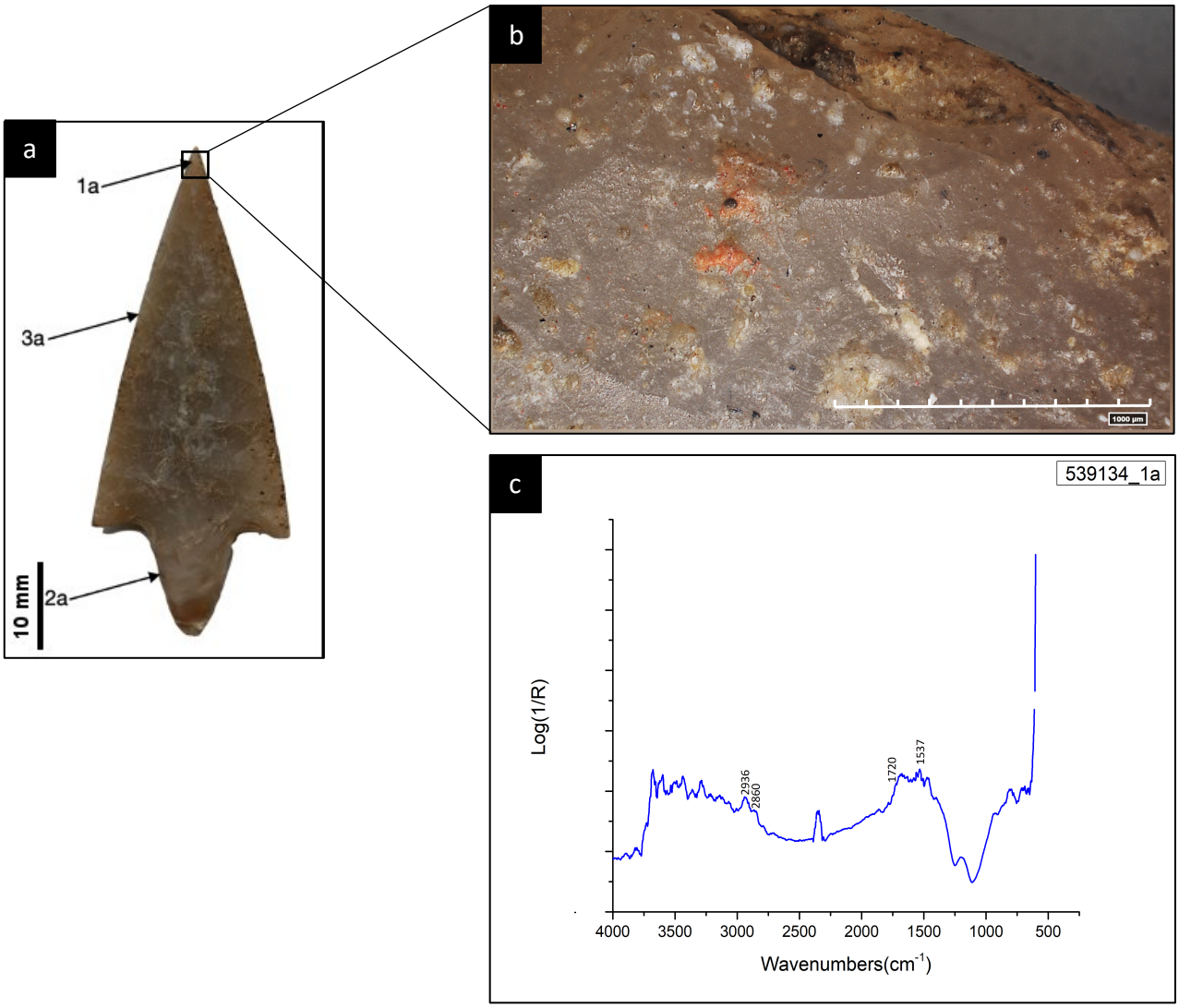


**Figure 11:** Tool number 539134 with residue results. (a) Tool number 539134 showing residue map. (b) Red pigment mixed with some sediments and whitish waxy residues (RLM Micrograph, 1000µm). (c) micro-FTIR spectrum of the residue

*1.2* Tool number 539134_5b

The results of the residue preserved on Tool number 539134 from Tomb 4 is showed in Figure 12. Residue 539134_5b is located on the proximal left part of the tool (Fig. 12a), preserved on the edge of the stone tool surface. The residues seem almost cemented on the stone tool surface along with sediments, red pigments and brown amorphous residues (Fig. 12b). The micro-FTIR spectrum show very weak peaks attributed to the C–H stretching at 2947 $cm^{-1}$ likely attributable to organic material. The prominent peaks observed within the spectral range of 3000 to 3800

cm $^{1}$, which are associated with the absorption of OH groups, can be attributed to the existence of water molecules located on the surface (Prinsloo, et al., 2014).

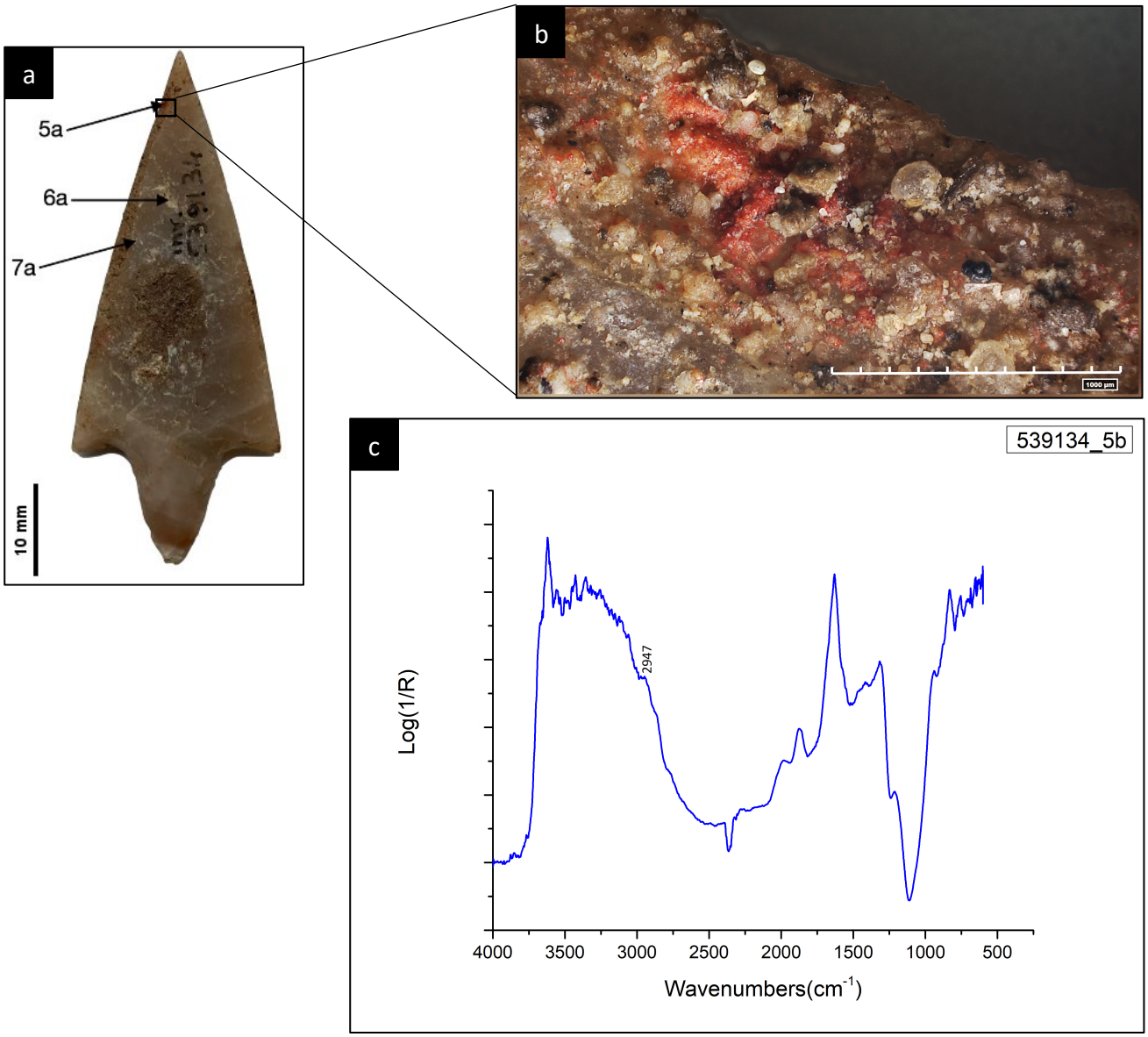


**Figure 12:** Tool number 539134 with residue results. (a) Tool number 539134 showing residue map. (b) Red pigment mixed with some sediments (RLM Micrograph, 1000µm). (c) micro-FTIR spectrum of the residue

*1.3* Tool number 538134_6a

The results of the residue preserved on Tool number 539134 from Tomb 4 is showed in Figure 13. Residue 539134_6a is located in the middle part of the tool oriented towards the proximal side (Fig. 13a). The residues are whitish, opaque and waxy in their texture which look very similar to fat residues (Fig. 13b). The micro-FTIR spectrum show some peaks attributed to the C–H stretching at 2935 cm$^{-1}$ and 2867 cm$^{-1}$ which shows the presence of organic material. In

the region between 1660 and 1573 $cm^{-1}$, amide I and II (Prinsloo, et al., 2014) bands can be seen overlapping with each other due to the rough, irregular surface and indicate the presence of protein.

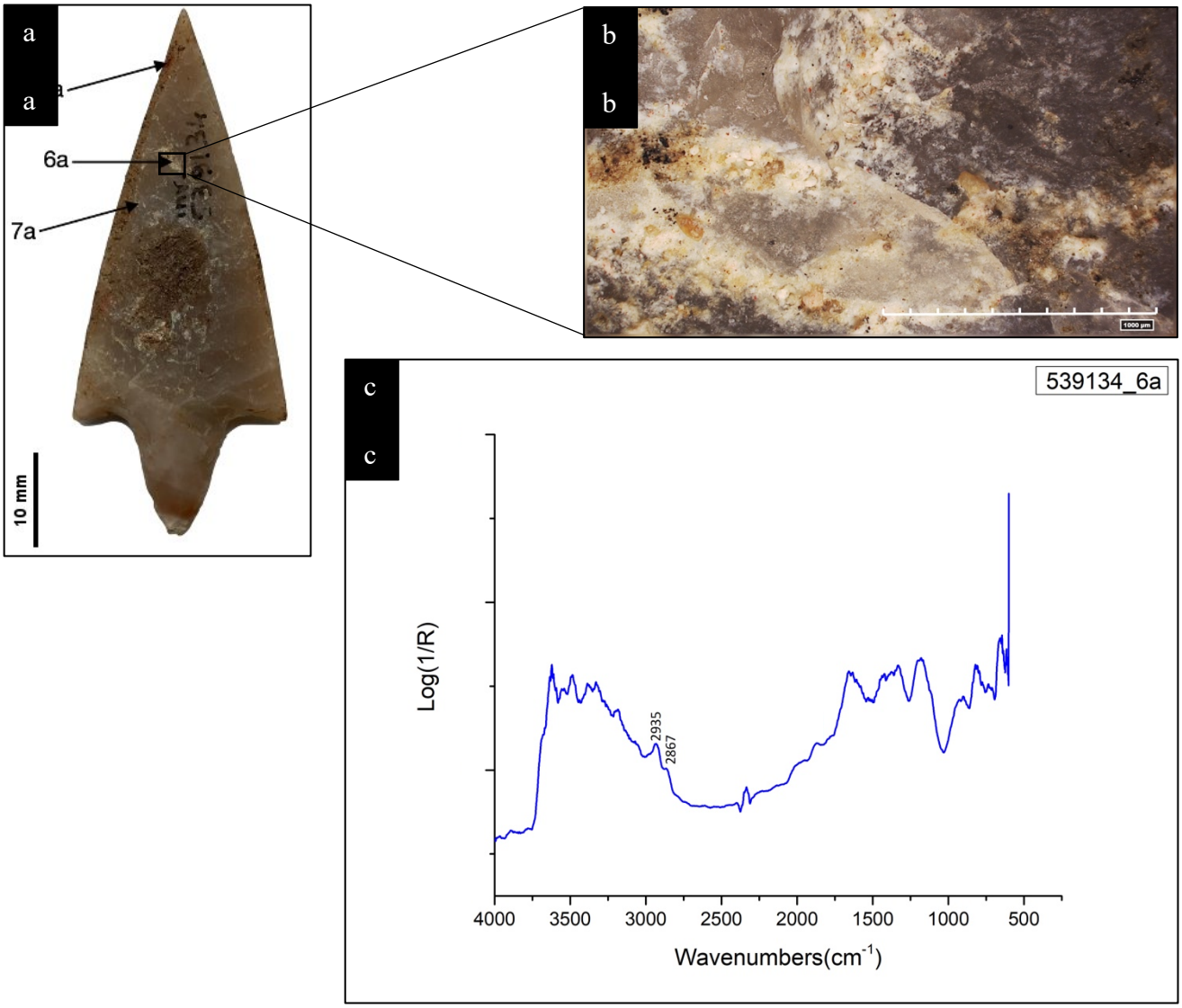


**Figure 13:** Tool number 539134 with residue results. (a) Tool number 539134 showing residue map. (b) White waxy residues mixed with some sediments (RLM Micrograph, 1000µm). (c) micro-FTIR spectrum of the residue

2. Tool number 539157

The results of Tool number 539157 from Tomb 4 are shown in Figure 14. Residue No. 539157_2a showed the presence of red pigments (Fig. 14b) on the surface of the stone tool. These pigments are not due to use, but rather seem to be sprinkled on the surface of the tool.

The EDX results show the presence of a high amount of Mercury in the spectrum confirming that the red pigments are Cinnabar (Guglielmi, et al., 2022).

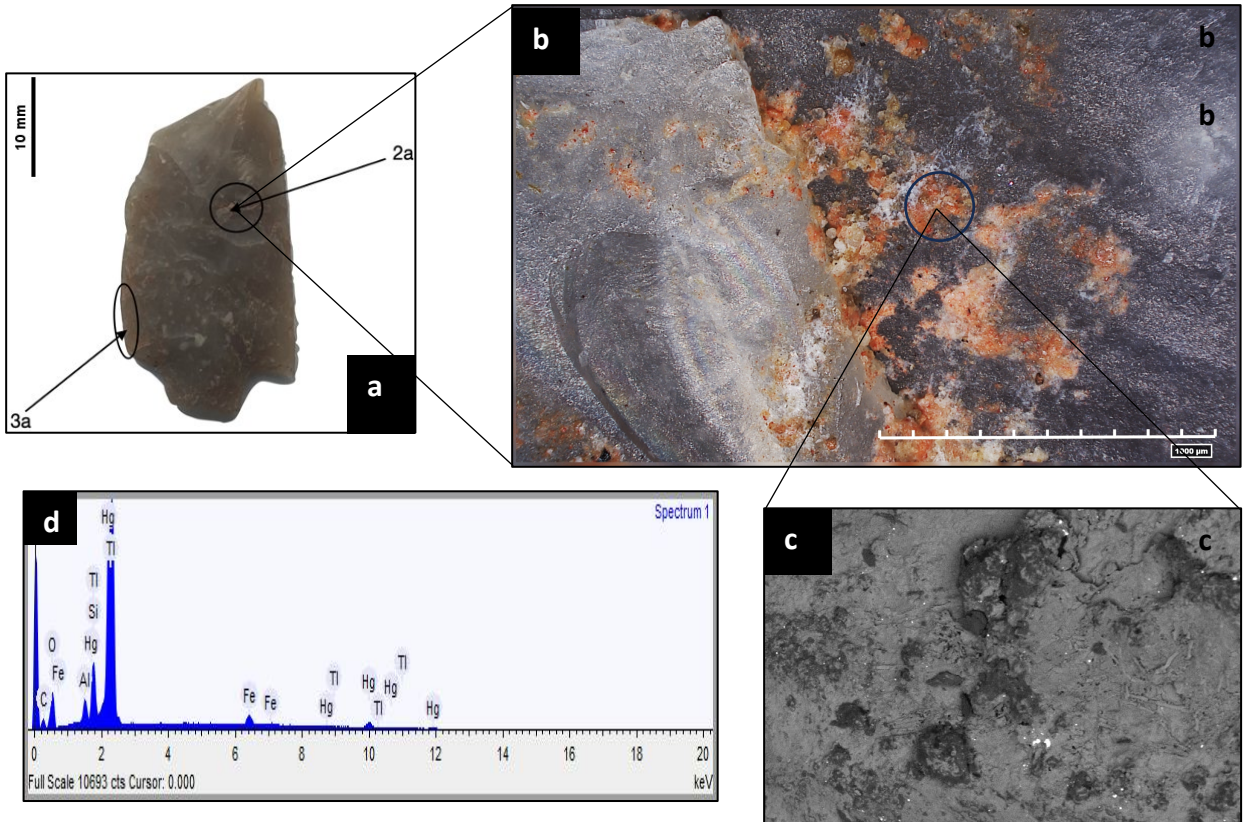


**Figure 14:** Tool number 539157 with residue results. (a) Tool number 539157 showing residue map. (b) Red pigments along with white amorphous residues (RLM micrograph, magnification 1000 µm. (c) BSE-SEM image showing close-up of the red pigments. (d) EDX spectrum of the red pigment

### *4.1.3 Tomb 5*

1. Tool number 539207

*1.1.* 539207_5b

The results of Tool number 539207 from Tomb 5 are shown in Figure 15. The residues are located in the middle part of the tool (Fig. 15a) and have an opaque whitish appearance with the presence of some sediments and fibres mixed together (Fig. 15b). The micro-FTIR spectrum (Fig. 15c) shows the presence of Amide A and Amide B at 3290 $cm^{-1}$ and 3082 $cm^{-1}$. The presence of organic residues is confirmed by the presence of C–H stretching at 2930 $cm^{-1}$ and 2859 $cm^{-1}$. The presence of lipids is confirmed due to the Carbonyl peak at 1715 $cm^{-1}$ (indicated by the arrow). The characteristic peaks of 1653 and 1593 $cm^{-1}$ attributable to the

Amide I and Amide II peaks respectively confirm the presence of proteinaceous material on the stone tool surface.

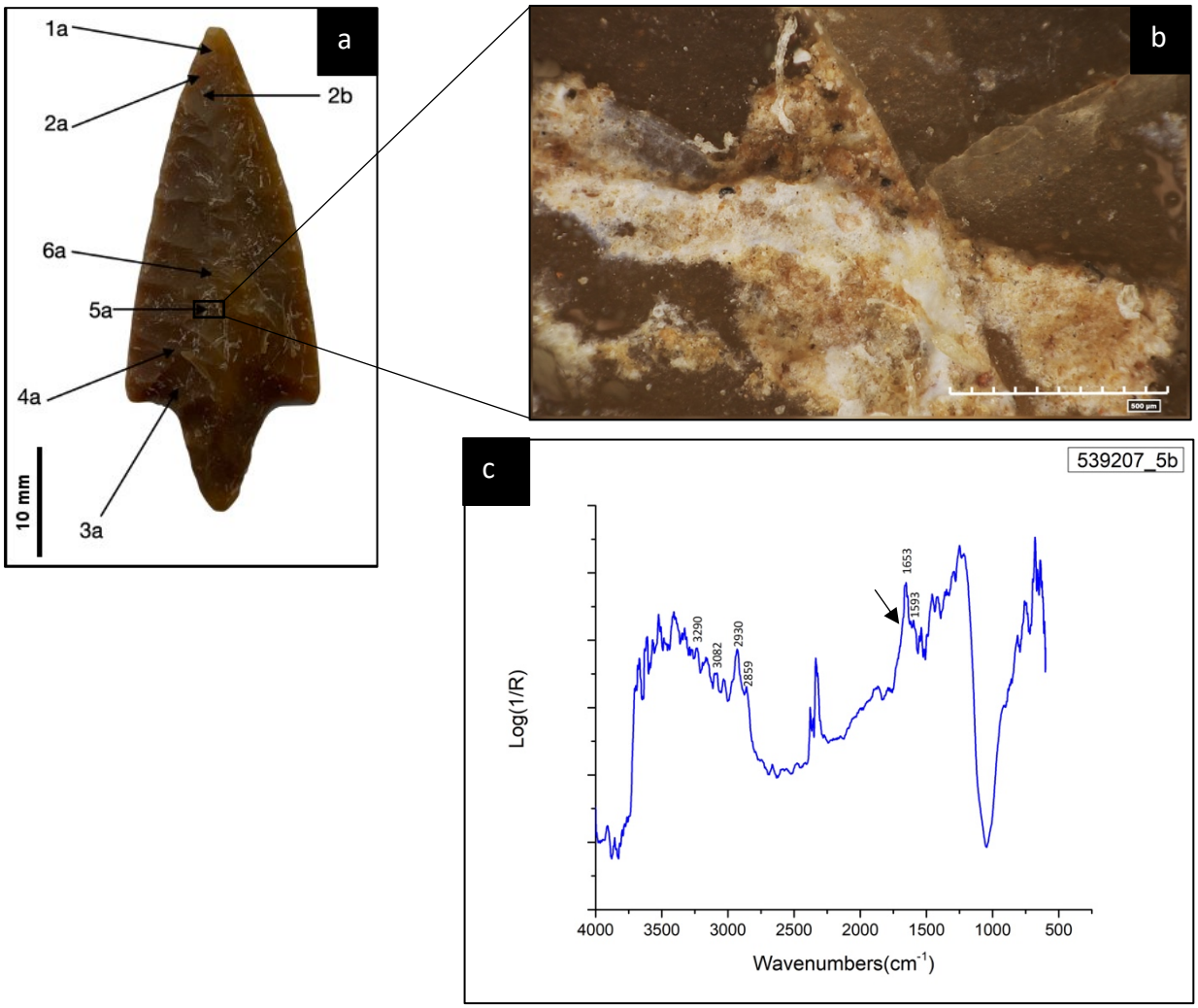


**Figure 15:** Tool number 539207 with residue results. (a) Tool number 539207 showing residue map. (b) White waxy residues mixed with some sediments and fibres (RLM Micrograph, 500µm). (c) micro-FTIR spectrum of the residue

*1.2.* Tool number 539207_8a

The results of Tool number 539207 from Tomb 5 are shown in Figure 16. The residue number 539207_8a is located on the proximal end of the tool (Fig. 16a). The residue is characterised by a white hue and some collagenous fibres along with sediments and a metallic spot in the middle (Fig. 16b). The micro-FTIR spectrum (Fig. 16c) shows the presence of organic residues due to the characteristic peaks attributable to C–H stretching at 2929 and 2875 $cm^{-1}$. The presence of proteinaceous material is confirmed due to weak peaks belonging to Amide I, II and III at 1624, 1581 and 1248 $cm^{-1}$ respectively.

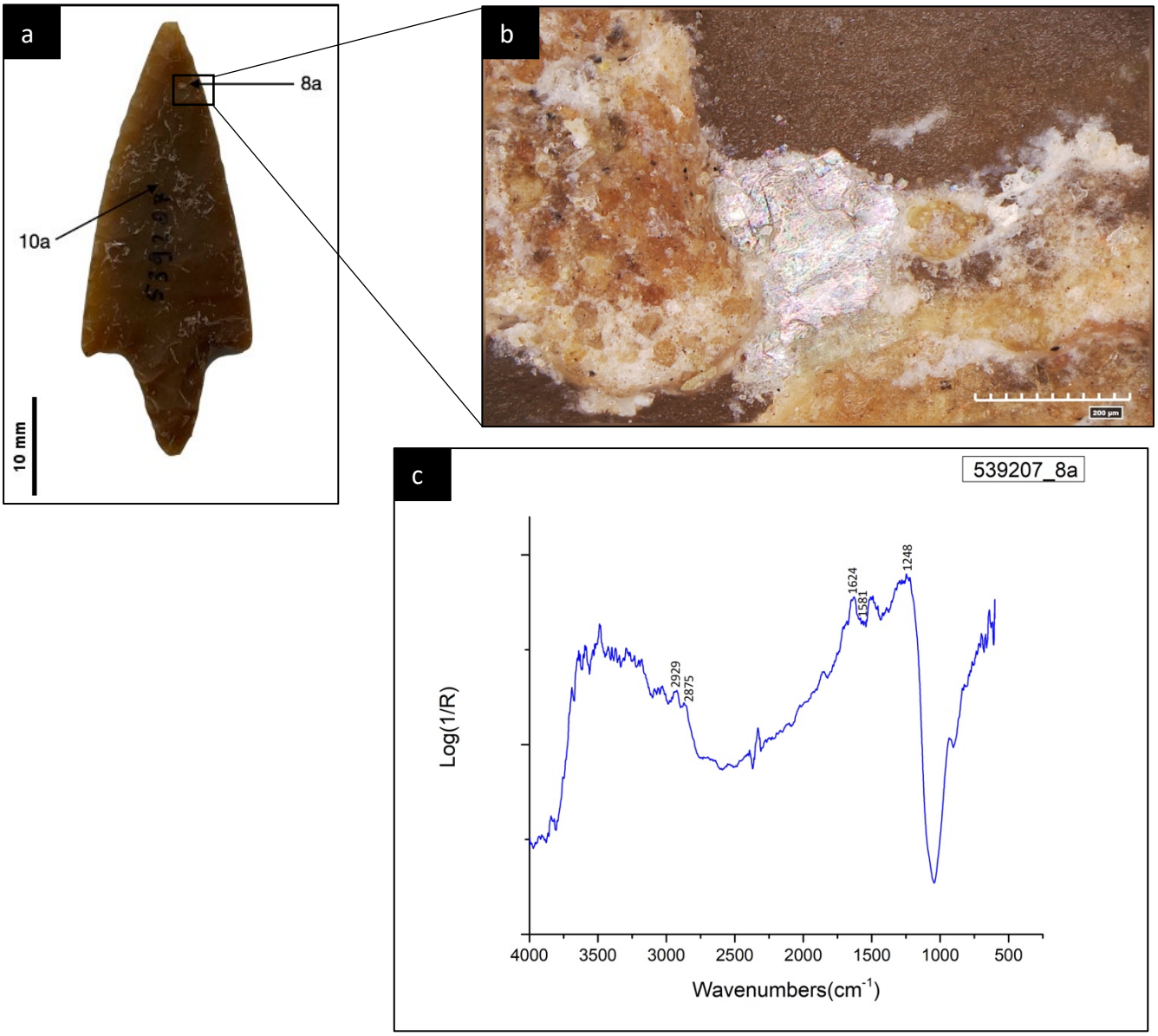


**Figure 16:** Tool number 539207 with residue results. (a) Tool number 539207 showing residue map. (b) White residues mixed with some sediments and fibres (RLM Micrograph, 200µm). (c) micro-FTIR spectrum of the residue

2. Tool number 539208

The results for Tool number 539208 from Tomb 5 are shown in Figure 17. The residue number 539208_3a is located on the middle part of the proximal end (Fig. 17a) and is characterised by brown amorphous residues along with fibres (Fig. 17b). The micro-FTIR spectrum (Fig. 17c) shows characteristics belonging to Amide A and B at 3467 and 3046 $cm^{-1}$ respectively. The presence of proteinaceous material is further confirmed due to the peaks at 1630 and 1584 $cm^{-1}$ attributable to Amide I and II.

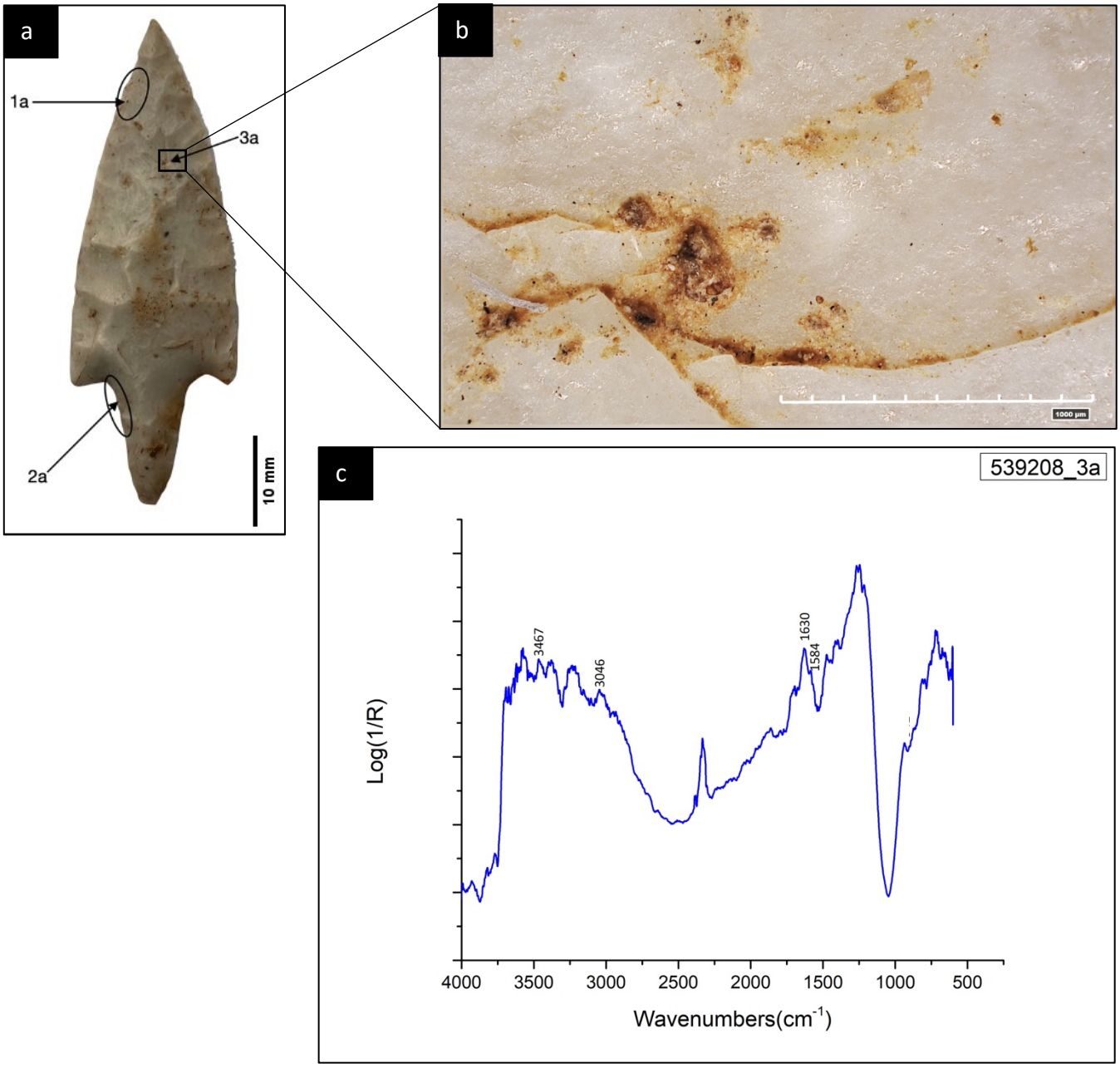


**Figure 17:** Tool number 539208 with residue results. (a) Tool number 539208 showing residue map. (b) Amorphous brown residues mixed with some sediments and fibres (RLM Micrograph, 1000µm). (c) micro-FTIR spectrum of the residue

3. Tool number 539210

The results of Tool number 539210 from Tomb 5 can be seen in Figure 18. The residues are located almost towards the distal end near the shoulder of the tang (Fig. 18a) and is characterised by a whitish, almost glassy appearance (Fig. 18b). The trail in the centre of the residue is probably due to some kind of microbial activity. The micro-FTIR spectrum (Fig. 18c) shows the presence of organic residues due to the peaks at 2931 and 2862 $cm^{-1}$ attributable to C–H stretching modes. The presence of proteinaceous materials is confirmed due to the Amide I and II peaks seen at 1676 and 1584 $cm^{-1}$.

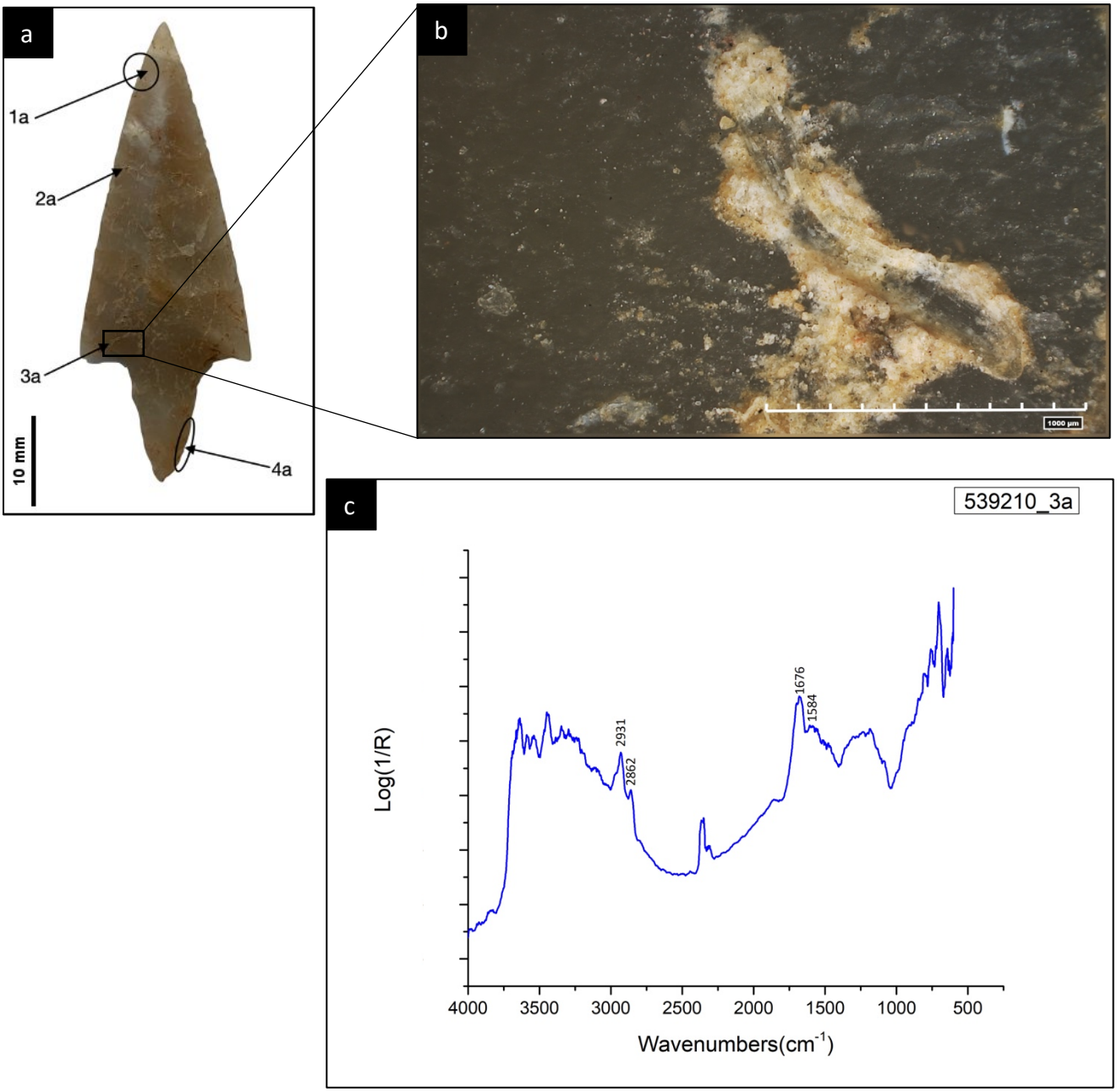


**Figure 18:** Tool number 539210 with residue results. (a) Tool number 539210 showing residue map. (b) Amorphous white residues (RLM Micrograph, 1000µm). (c) micro-FTIR spectrum of the residue

4. Tool number 539215

The results from Tool number 539215 from Tomb 5 are shown in Figure 19. The residues are located on the distal end of the tool very close to the shoulder of the tang (Fig. 19a). The residues are in a whitish-yellowish hue and present a wax-like appearance (Fig. 19b). The micro-FTIR spectrum (Fig. 19c) show the presence of organic residues due to the presence of C–H stretching mode observed at 2950 and 2852 $cm^{-1}$. The shoulder at 1722 $cm^{-1}$ is due to the Carbonyl group and shows the presence of fat in the residue. Proteinaceous materials are

confirmed due to the presence of Amide I and II peaks at 1688 and 1543 $cm^{-1}$. The peak at 1441 $cm^{-1}$ is attributed to the $CH_x$ bending modes.

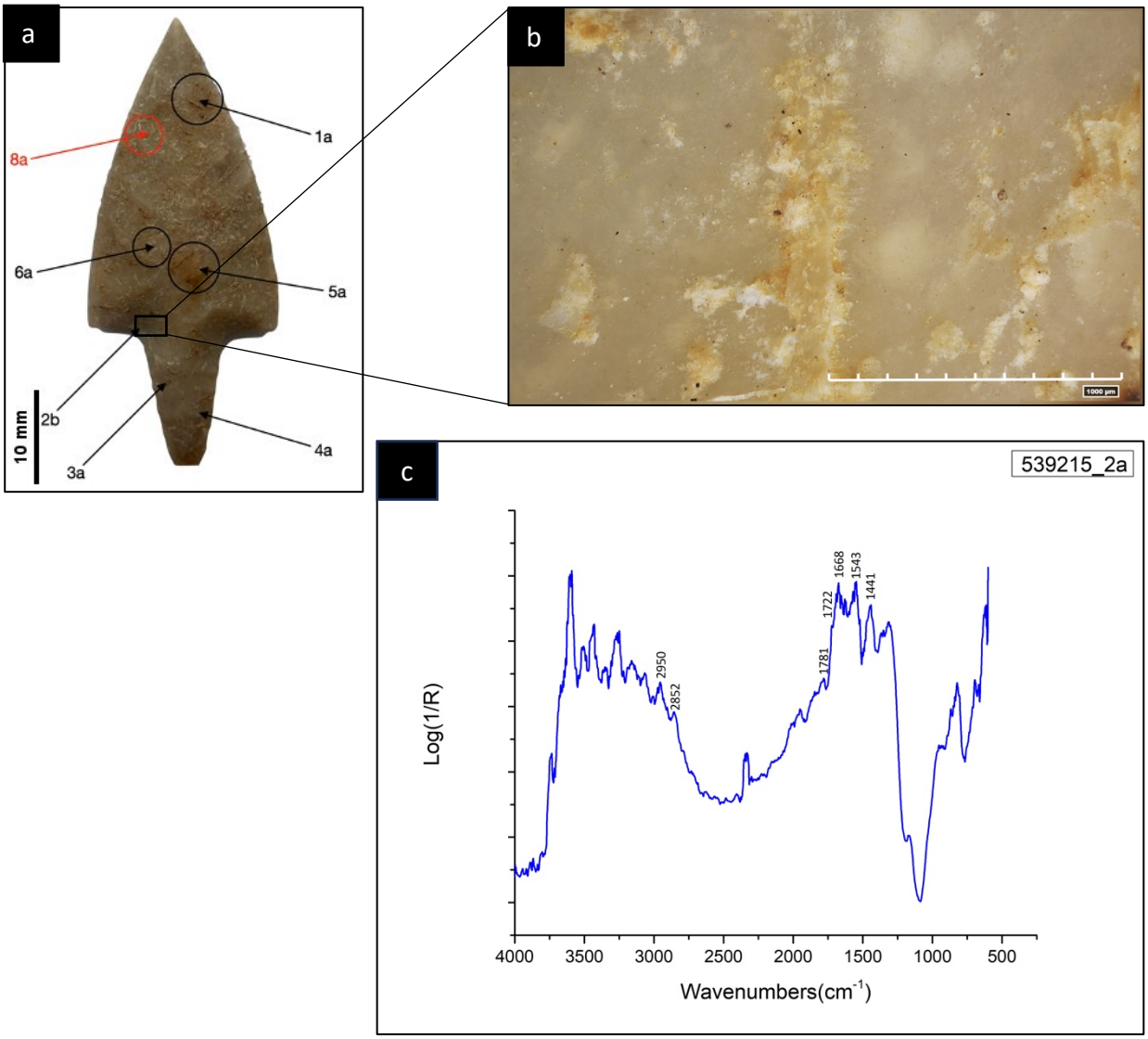


**Figure 19:** Tool number 539215 with residue results. (a) Tool number 539215 showing residue map. (b) Yellowish waxy residues (RLM Micrograph, 1000µm). (c) micro-FTIR spectrum of the residue

5. Tool number 539220

The results for Tool number 539220 from Tomb 4 are shown in Figure 20. The residues are located towards the distal end on the shoulder of the tang (Fig. 20a). White amorphous residues along with some fibres are located on the stone tool surface in small lumps (Fig. 20b). The presence of organic materials can be seen in the micro-FTIR (Fig. 20c) with peaks at 2924 and 2859 $cm^{-1}$ attributable to the C–H stretching modes. The peaks at 1630 and 1544 $cm^{-1}$ are attributed to the Amide I and II group and indicate the presence of proteinaceous materials.

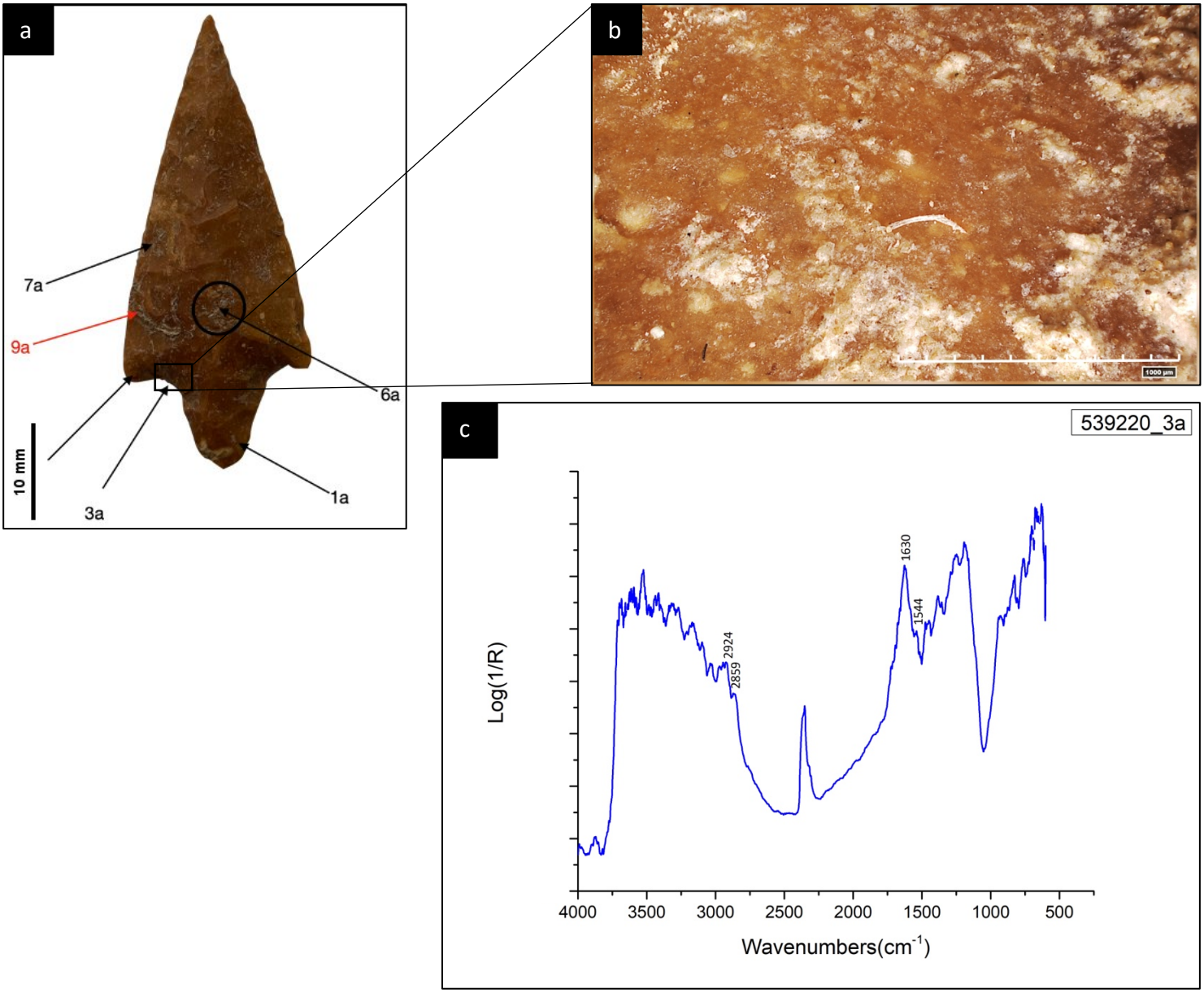


**Figure 20:** Tool number 539220 with residue results. (a) Tool number 539220 showing residue map. (b) White amorphous residues with fibres (RLM Micrograph, 1000µm). (c) micro-FTIR spectrum of the residue

6. Tool number 539222

The results from Tool number 539222 from Tomb 5 are shown in Figure 21. The residues are situated on the edge of the tool (Fig. 21a) and are yellowish in colour (Fig. 21b) and seem to be almost cemented on the edge of the stone tool surface. The micro-FTIR results show characteristic peaks at 2928 and 2865 $cm^{-1}$ attributable to the C–H stretching modes which indicate the presence of organic resides on the tool.

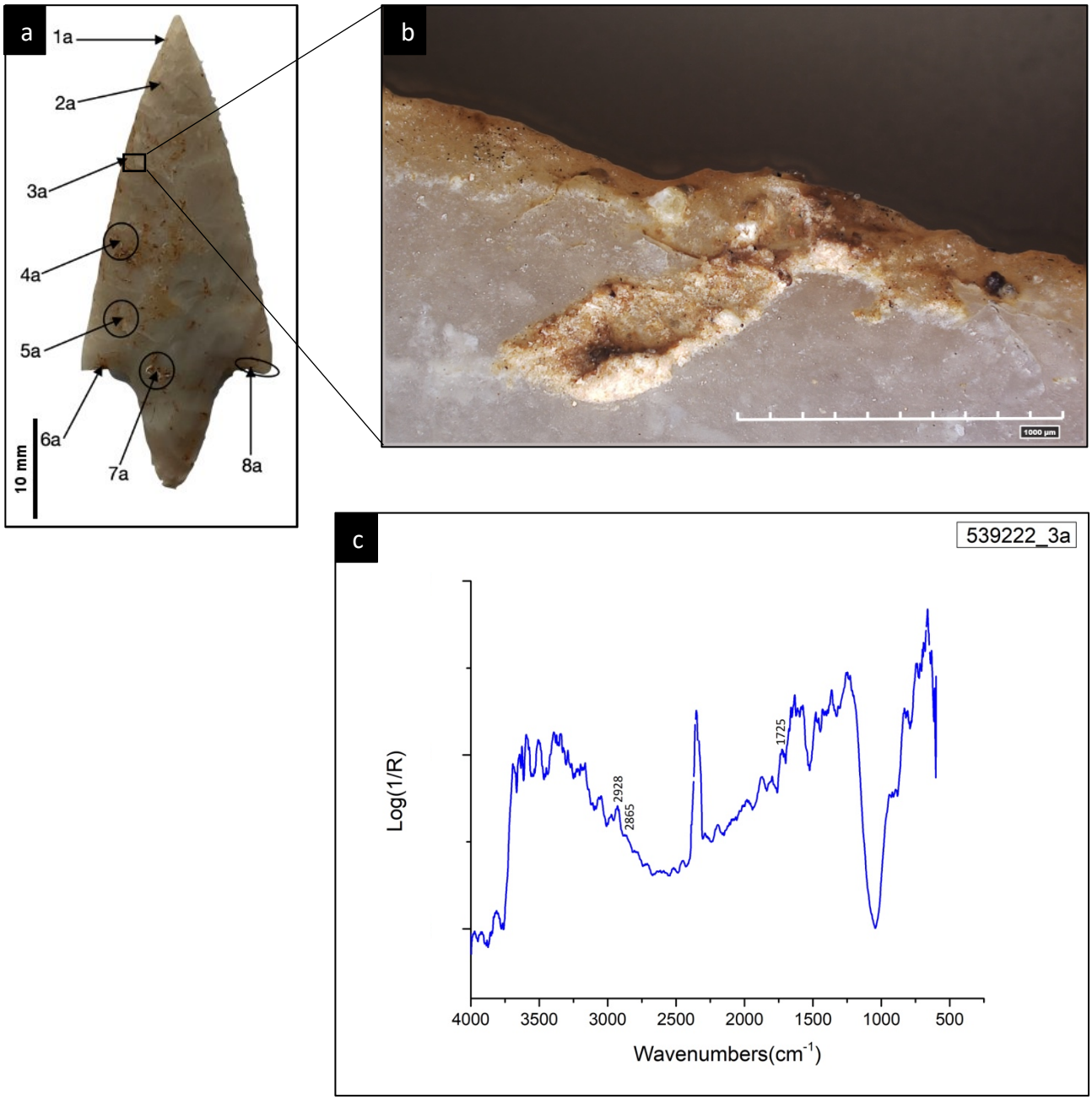


**Figure 21:** Tool number 539222 with residue results. (a) Tool number 539222 showing residue map. (b) Whitish-yellowish amorphous residues with sediments (RLM Micrograph, 1000µm). (c) micro-FTIR spectrum of the residue

7. Tool number 539223

The results for the Tool number 539223 from Tomb 5 are shown in Figure 22. The residues are located on the edge of the tool (Fig. 22a) and have been preserved in the micro-fractures and are situated towards the proximal end of the tool. Brownish amorphous residues mixed with sediments can be seen located in small lumps (Fig. 22b). The micro-FTIR spectrum (Fig. 22c) is distorted due to the interreference of the stone surface, but some organic materials can still

be seen. Peaks 2940 and 2865 $cm^{-1}$ attributed to the C–H stretching modes reveal the occurrence of organic residues.

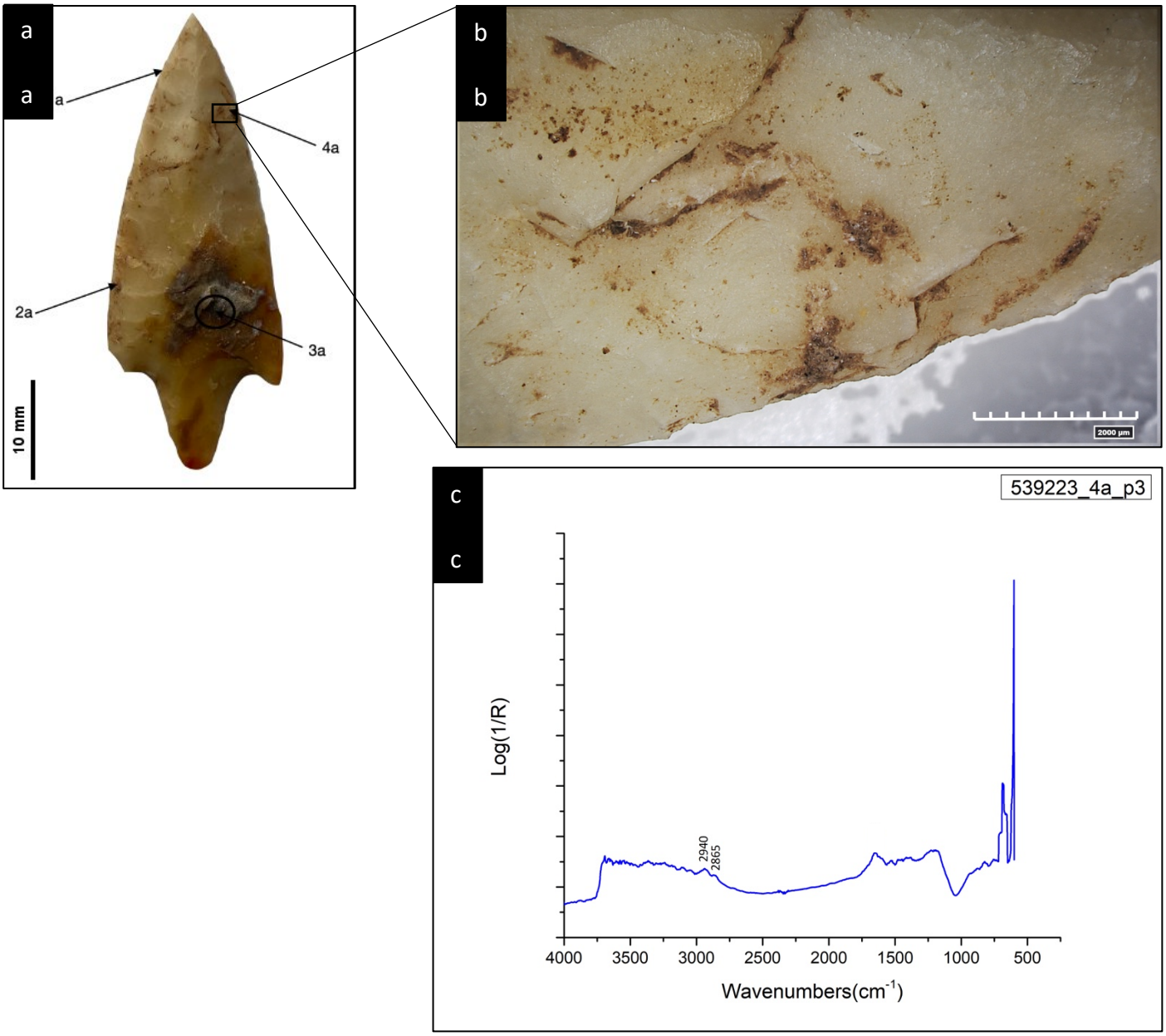


**Figure 22:** Tool number 539223 with residue results. (a) Tool number 539223 showing residue map. (b) Brown amorphous residues with sediments and fibres (RLM Micrograph, 2000µm). (c) micro-FTIR spectrum of the residue

8. Tool number 539224

The results for Tool number 539224 from Tomb 5 are shown in Figure 23. The residues are located near the edge of the tool (Fig. 23a) and are characterised by brownish-whitish amorphous features (Fig. 23b). The micro-FTIR spectrum (Fig. 23c) shows peaks attributable to C–H stretching modes at 2931 and 2861 $cm^{-1}$ confirming the presence of organic residues.

The shoulder at 1721 $cm^{-1}$ can be attributed to the carbonyl group. The peak at 1454 $cm^{-1}$ is attributed to the $CH_x$ bending modes.

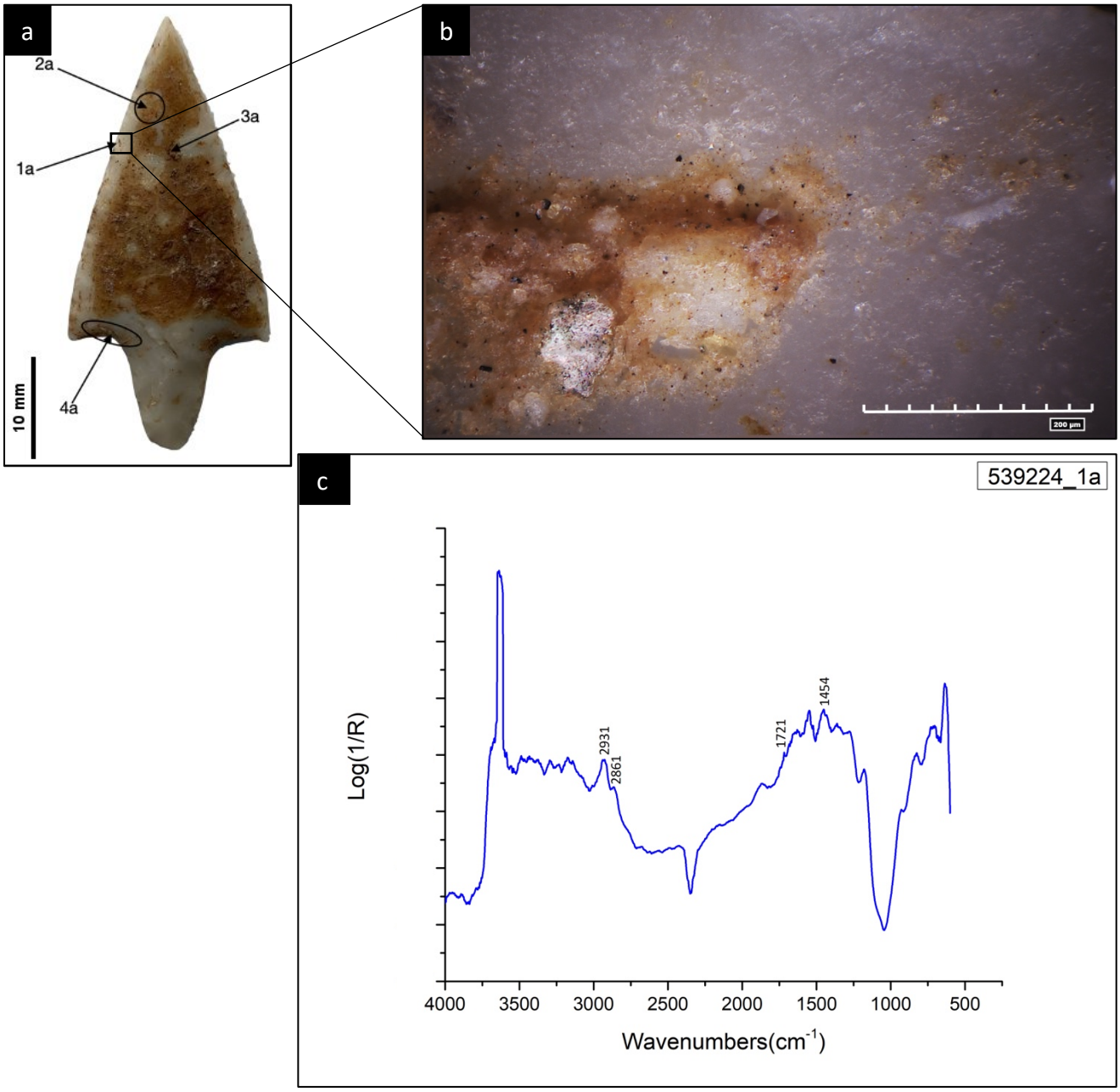


**Figure 23:** Tool number 539224 with residue results. (a) Tool number 539224 showing residue map. (b) Brownish- whitish amorphous residues (RLM Micrograph, 200µm). (c) micro-FTIR spectrum of the residue

### *4.1.4 Tomb 7*

1. Tool number 539190

*1.1.* 539190_1b

The results for Tool number 539190 from Tomb 7 are shown in Figure 24. The residues are located on the edge of the tool towards the proximal end (Fig. 24a). The residues are

yellowish in colour (Fig. 24b) and are of an amorphous nature. The micro-FTIR spectrum (Fig. 24c) exhibits peaks at 2936 and 2860 $cm^{-1}$ which are attributable to C–H stretching modes and show the presence of organic residues.

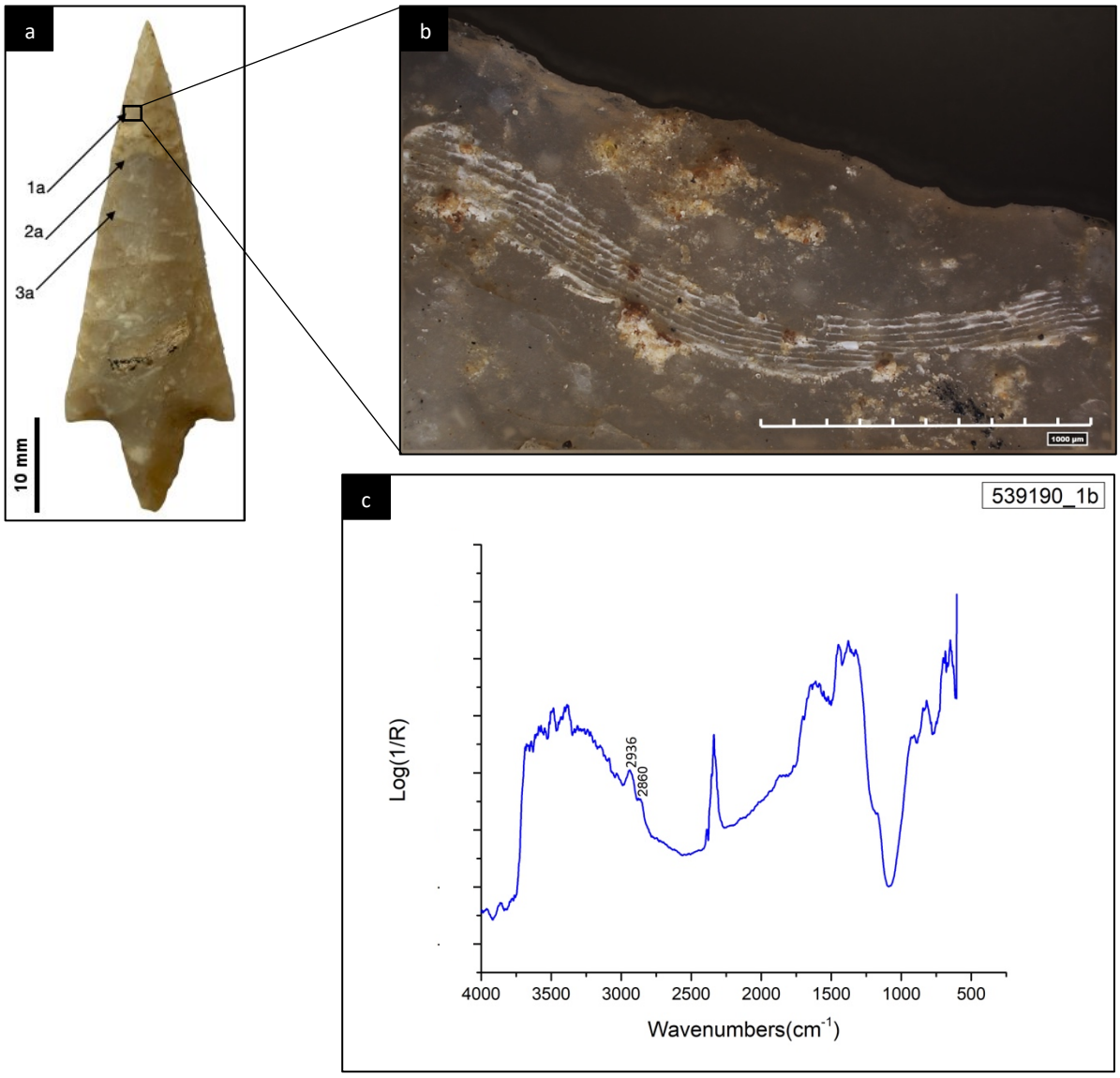


**Figure 25:** Tool number 539190 with residue results. (a) Tool number 539190 showing residue map. (b) Yellowish amorphous residues (RLM Micrograph, 1000µm). (c) micro-FTIR spectrum of the residue

### *1.2.* 539190_6a

The results of Tool number 539190 from Tomb 7 are shown in Figure 25. The residues are located near the edge in the middle part of the tool (Fig. 25a). The residues are of an amorphous nature (Fig. 25b) and are yellowish whitish in hue. The results from the micro-FTIR analysis show peaks at 2941 and 2859 $cm^{-1}$ (Fig. 25c) which are attributed to the C–H stretching modes and reveal the presence of organic residues on the sample.

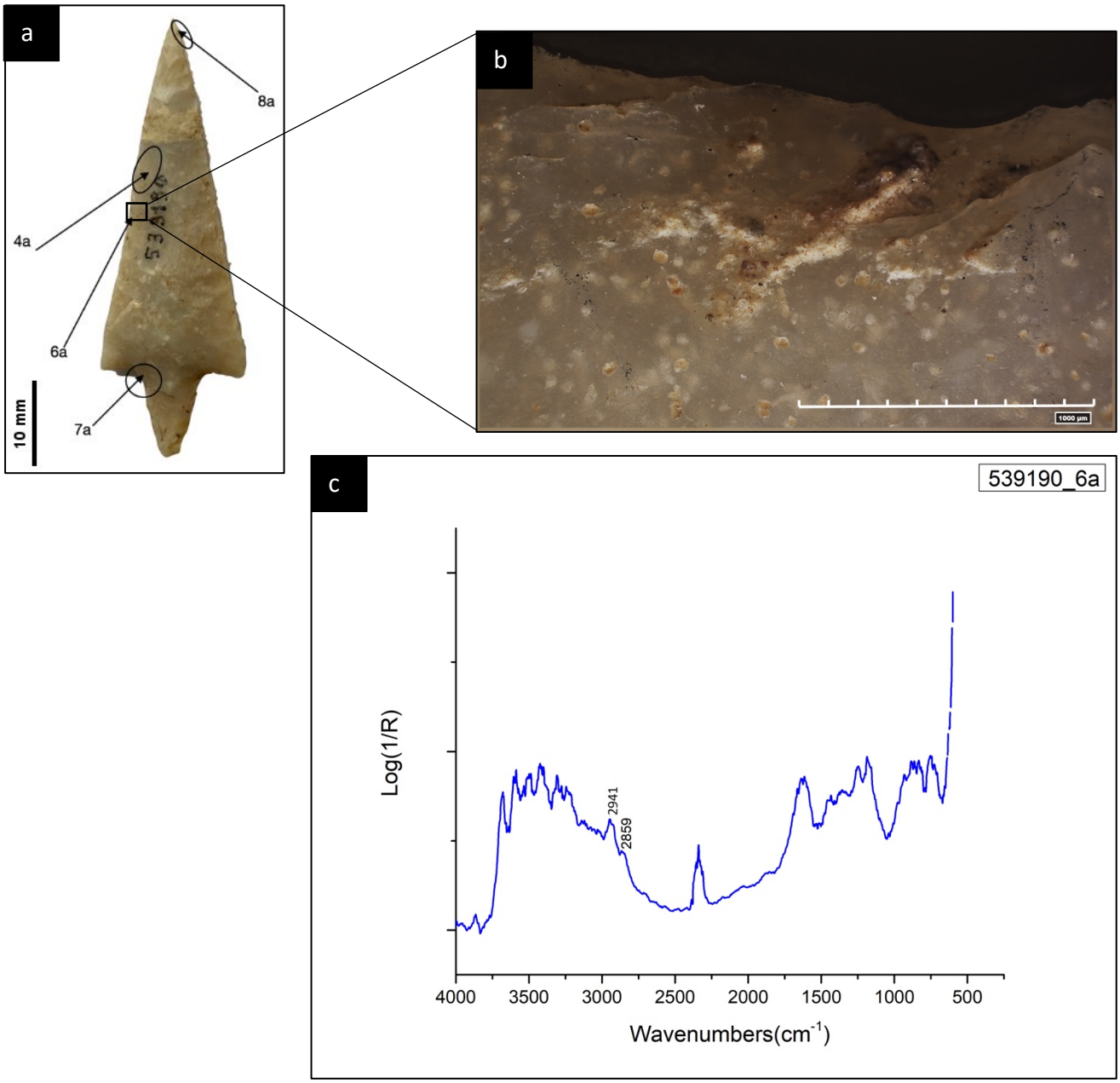


**Figure 26:** Tool number 539190 with residue results. (a) Tool number 539190 showing residue map. (b) Yellowish amorphous residues (RLM Micrograph, 1000µm). (c) micro-FTIR spectrum of the residue

2. Tool number 539192

*2.1.* 539192_4a

The results of Tool number 539192 from Tomb 7 are shown in Figure 26. The residues are located on the shoulder part of the tang (Fig. 26a) towards the distal end. The residues are of an amorphous nature and are spread in a powdery form along with some sediments (Fig. 26b). The SEM image show some organic residues which show up dark grey (Fig. 26c) against a light background, along with the sediments and some phytoliths. The EDX

spectrum shows a high amount of Bromine present in the residue (Fig. 26d) which cannot be explained as of now. The micro-FTIR results (Fig. 26e) exhibit characteristic peaks at 2931 and 2861 $cm^{-1}$ which are attributed to the C–H stretching modes and show the presence of organic residues. The peaks at 1635 and 1588 $cm^{-1}$ are attributed to Amides I and II group and reveal the presence of proteinaceous material in the sample.

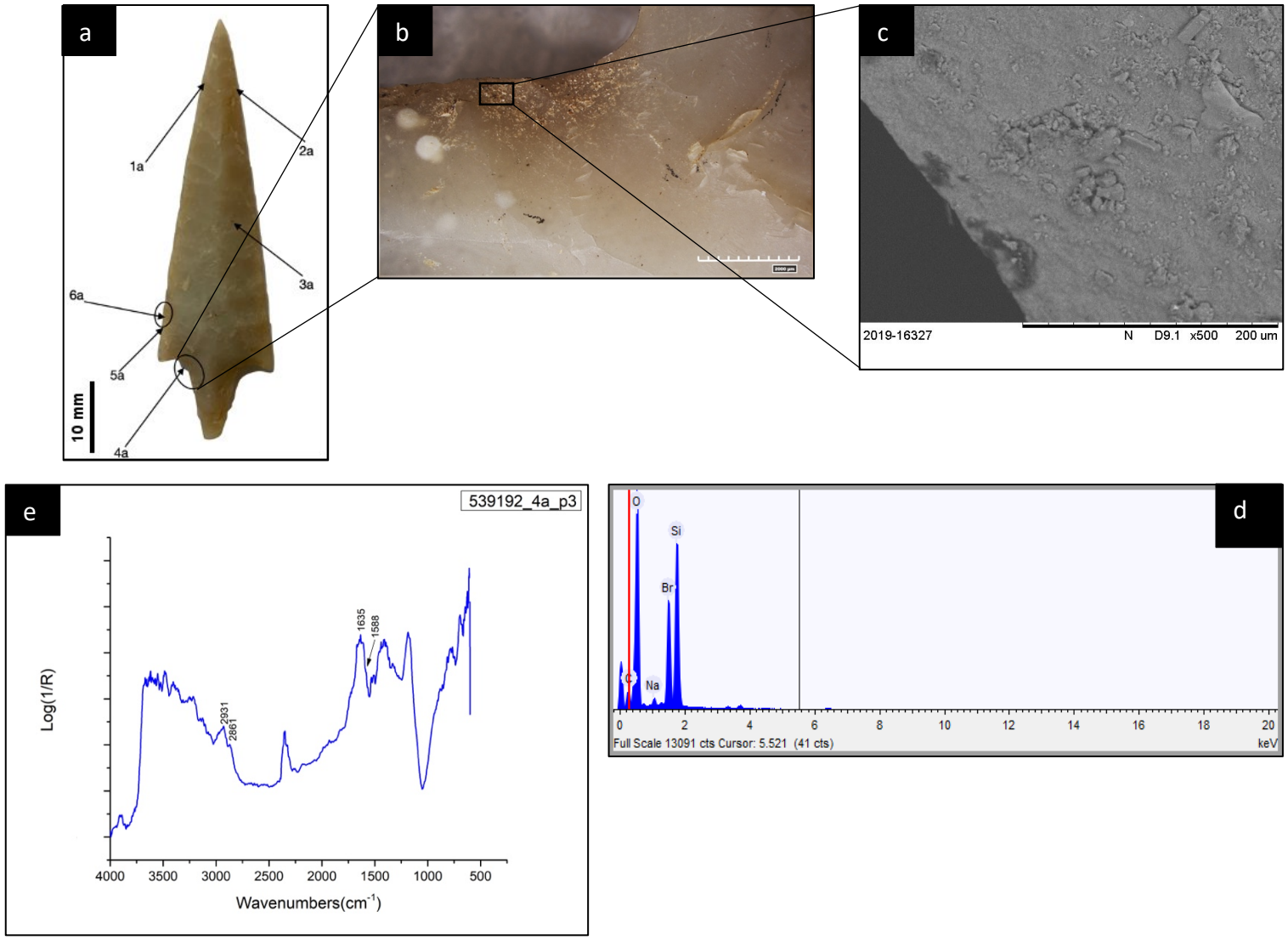


**Figure 27:** Tool number 539192 with residue results. (a) Tool number 539192 showing the residue map. (b) Powdery white amorphous residues along with sediments (RLM micrograph, magnification: 2000 μm. (c) Residues along with sediments (BSE-SEM image). (d) EDX spectrum of the residue. (e) micro-FTIR spectrum of the residue

*2.2.* 539192_10a

The results of Tool number 539192 from Tomb 7 can be seen in Figure 27. The residues are situated in the shoulder part of the tang (Fig. 27a) towards the distal end of the tool. The residues are white in colour and appear to be squelched (Fig. 27b) due to some activity. The

micro-FTIR results (Fig. 27c) exhibit peaks at 2927 and 2868 $cm^{-1}$ attributed to C–H stretching modes and reveal the presence of organic residues. The Amide I and II peaks at 1628 and 1580 cm-1 respectively show the presence of proteinaceous material in the sample.

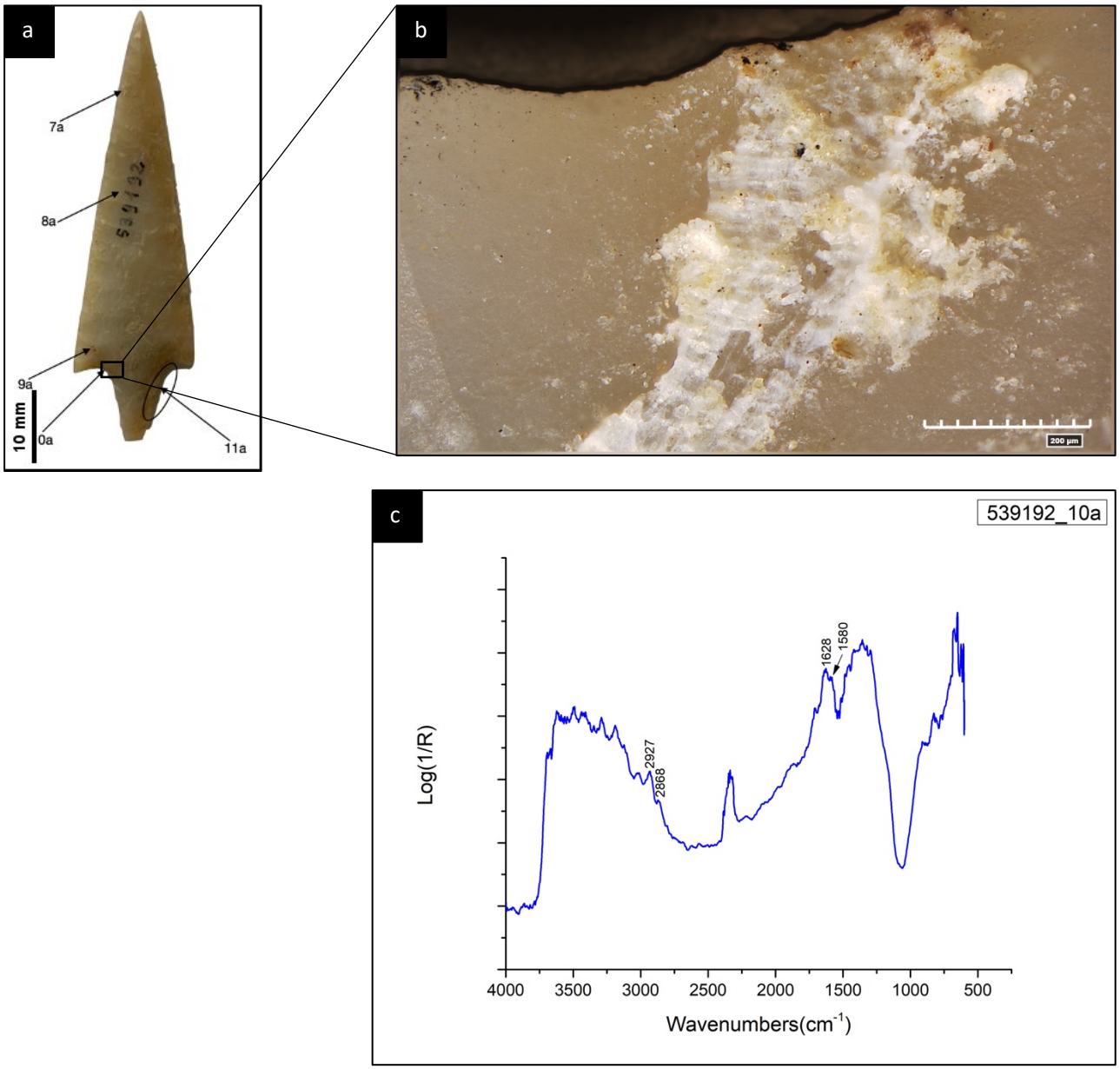


**Figure 28:** Tool number 539192 with residue results. (a) Tool number 539192 showing residue map. (b) Whitish amorphous residues (RLM Micrograph, 200µm). (c) micro-FTIR spectrum of the residue

3. Tool number 539195

The results of Tool number 539195 from Tomb 7 are shown in Figure 28. The residues are located on the edge of the tool (Fig. 28a) towards the proximal end. Yellowish amorphous residues can be seen (Fig. 28b) spread in a thin layer along with sediments. The micro-FTIR

results (Fig. 28c) show characteristic peaks at 2926 and 2855 $cm^{-1}$ attributed to the C–H stretching modes which reveal the presence of organic residues on the sample.

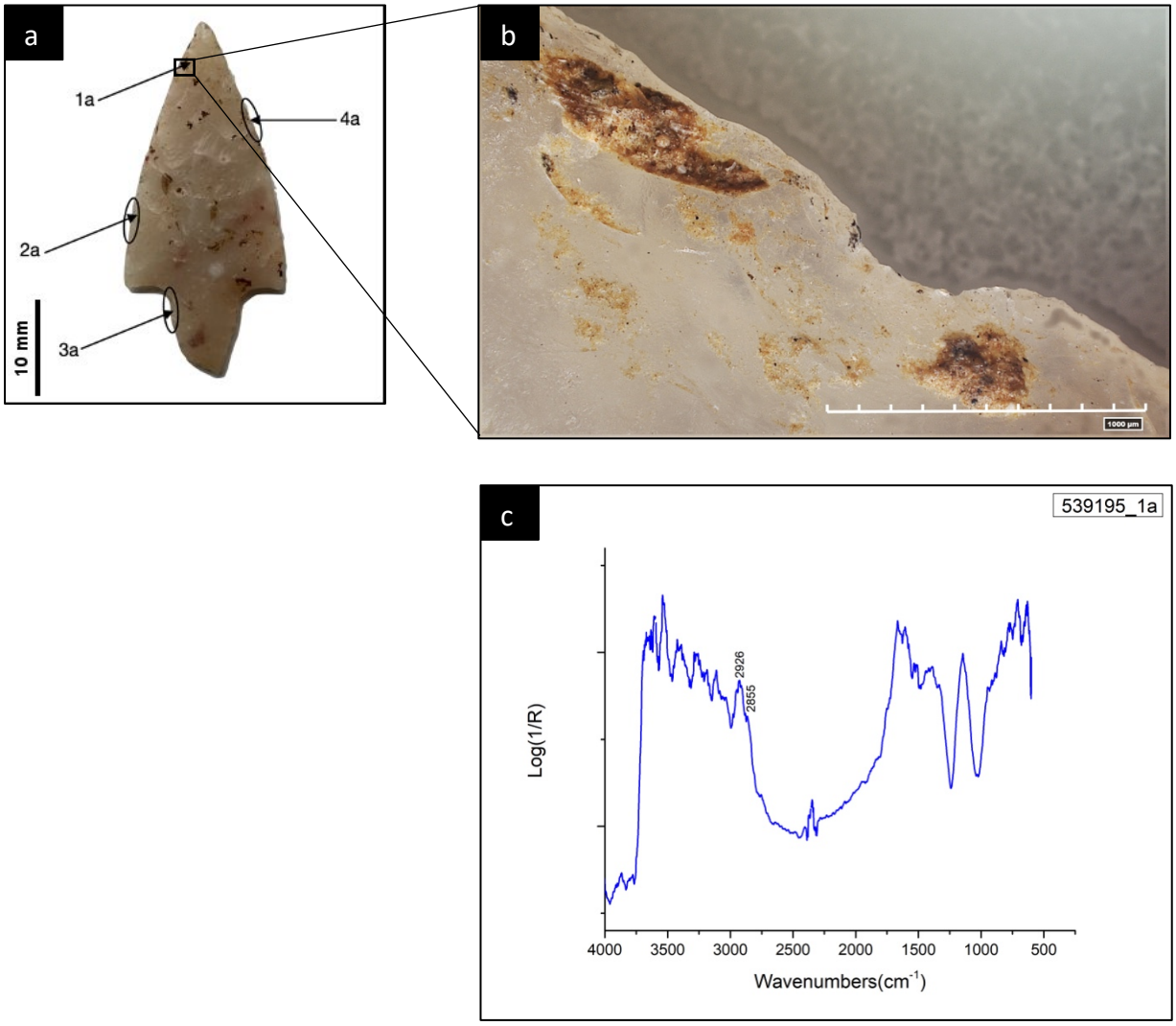


**Figure 29:** Tool number 539195 with residue results. (a) Tool number 539195 showing residue map. (b) Yellowish amorphous residues along with sediments (RLM Micrograph, 1000µ). (c) micro-FTIR spectrum of the residue

### *4.1.5 Tomb 14*

1. Tool number 539178

*1.1.* 539178_1b

The findings of the study of the residue preserved on Tool number 539178 from Tomb 14 are displayed in Figure 29. The micrograph of residue no. 1b is displayed in figure 29b, and it reveals dark amorphous residues in addition to sediments and some fibres. Additional SEM examination (Fig. 29c) reveals the presence of bone pieces that have been embedded

within the sediments. The existence of bone may also be verified by doing an EDX study (Fig. 29d), which reveals the presence of phosphorous and calcium. These elements are the primary constituents of hydroxyapatite, an inorganic mineral that accounts for 70 percent of bone's composition. The remaining thirty percent of bone is made up of organic substances, the majority of which are proteins, the most abundant of which is collagen (Prinsloo, et al., 2014). These findings are supported by the findings of the micro-FTIR analysis (Fig. 29e), which reveals the signature peaks of Amide I at 1679 $cm^{-1}$ and Amide II at 1578 $cm^{-1}$, both of which are characteristic of proteins. The existence of the C-H stretching mode at 2961 $cm^{-1}$ is additional evidence that organic residues are still present in the sample.

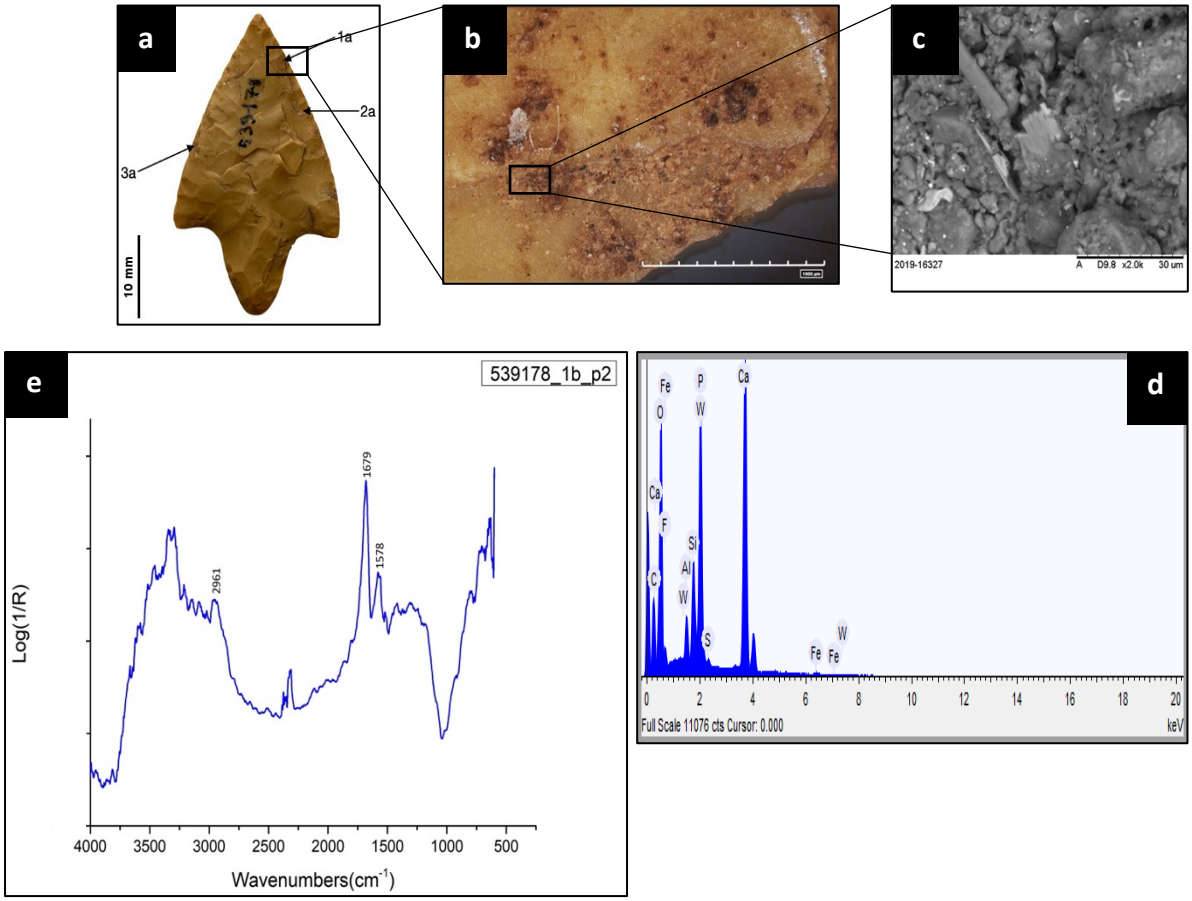


**Figure 30:** Tool number 539178 with residue results. (a) Tool number 539178 showing the residue map. (b) Brown amorphous residues along with sediments and fibres (RLM micrograph, magnification: 1000 µm. (c) Bone fragment embedded in sediments (BSE-SEM image). (d) EDX spectrum of the bone fragment. (e) micro-FTIR spectrum of the bone fragment.

### *1.2.* 539178_3b

The results of Tool number 539178 from Tomb 14 are displayed in Figure 30. The results are located on the edge of the tool in the middle portion (Fig. 30a). Brown amorphous

residues can be seen (Fig. 30b) along with sediments and fibres. The SEM image (Fig. 30c) shows a closer look at the fibres trapped within the sediments. The micro-FTIR results exhibit characteristic peaks at 2930 and 2863 cm-1 attributable to the C-H stretching modes and reveal the presence of organic residues. The Amide I and II peaks at 1653 and 1589 cm-1 show the occurrence of proteinaceous materials in the sample.

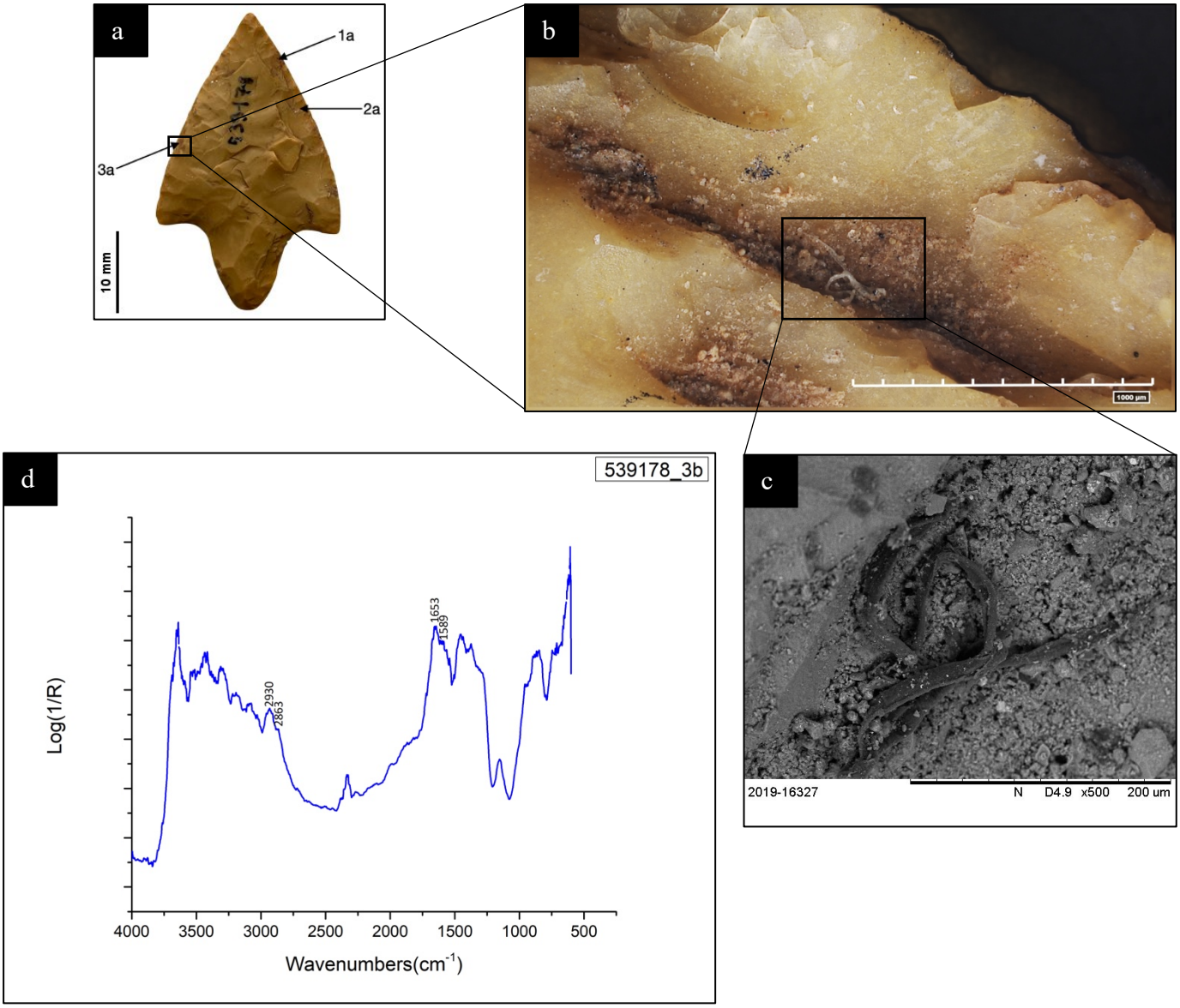


**Figure 31:** Tool number 539178 with residue results. (a) Tool number 539178 showing the residue map. (b) Brown amorphous residues along with sediments and fibres (RLM micrograph, magnification: 1000 µm. (c) Fibre embedded in sediments (BSE-SEM image). (d) micro-FTIR spectrum of the residue

2. Tool number 539179

*2.1.* 539179_3a

The results of the residue analysis of Tool number 539179 from Tomb 14 are displayed in Figure 31. The residues are situated on the edge of the shoulder of the tang towards the distal end (Fig. 31a) and are dark and amorphous in nature (Fig. 31b) along with sediments and fibres (Fig. 31c). The micro-FTIR results (Fig. 31d) show characteristic peaks at 2934 and 2874 $cm^{-1}$ attributed to the C-H stretching modes and show the presence of organic residues. A shoulder at 1720 $cm^{-1}$ shows the presence of carbonyl group. Characteristic Amide I and II peaks can be seen at 1641 and 1535 $cm^{-1}$ and reveal the presence of proteinaceous materials.

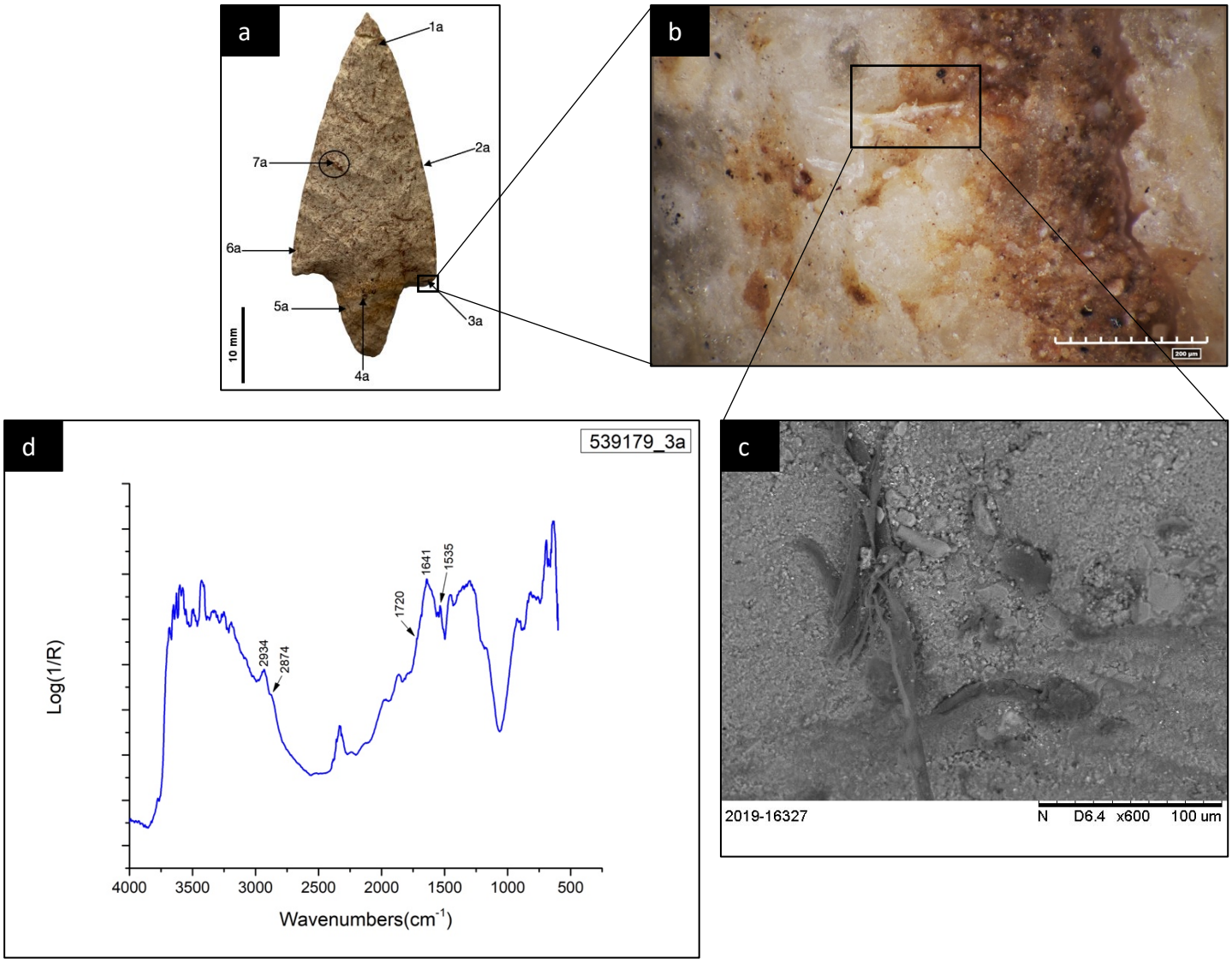


**Figure 32:** Tool number 539179 with residue results. (a) Tool number 539179 showing the residue map. (b) Brown amorphous residues along with sediments and fibres (RLM micrograph, magnification: 200 µm. (c) Fibre embedded in sediments (BSE-SEM image). (d) micro-FTIR spectrum of the residue.

*2.2.* 539179_12a

The results of Tool number 539179 from the Tomb 14 are displayed in Figure 32. The results are located near the shoulder of the tang towards the distal end (Fig. 32a). A black patch of residue surrounded by sediments and some fibres can be seen (Fig. 32b). The micro-FTIR results (Fig. 32c) show characteristic peaks at 2943 and 2868 $cm^{-1}$ attributed to C-H stretching modes. Amide I and II peaks can be seen at 1655 and 1535 $cm^{-1}$ revealing the presence of proteinaceous materials in the sample.

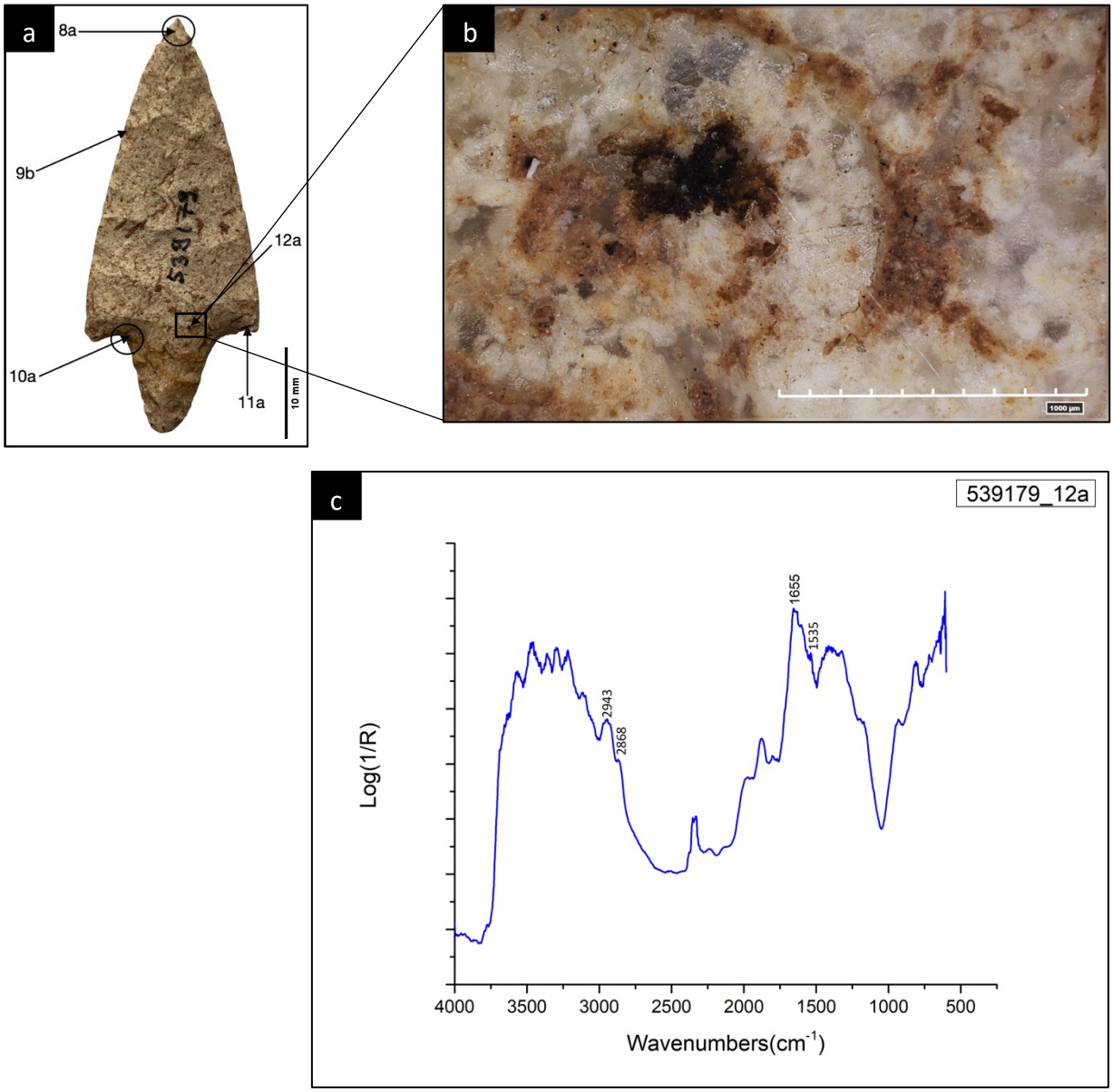


**Figure 33:** Tool number 539179 with residue results. (a) Tool number 539179 showing residue map. (b) Brown amorphous residues along with sediments, fibres and a black spot (RLM Micrograph, 1000µm). (c) micro-FTIR spectrum of the residue

3. Tool number 539180

The results of residue analysis for Tool number 539180 from Tomb 14 can be seen in Figure 33. The residues are situated on the distal end of the tool, right on the tip of the tang (Fig. 33a). The residues are dispersed in a random manner (Fig. 33b) and there appears to be some kind of sheen along with brown residues. The micro-FTIR results exhibit characteristic peaks at 2926 and 2855 $cm^{-1}$ attributed to C-H stretching modes and reveals the presence of organic residues. A shoulder belonging to the carbonyl stretch can be seen at 1720 $cm^{-1}$. Characteristic Amide I and II peaks are seen at 1664 and 1574 $cm^{-1}$ and show the presence of proteinaceous materials.

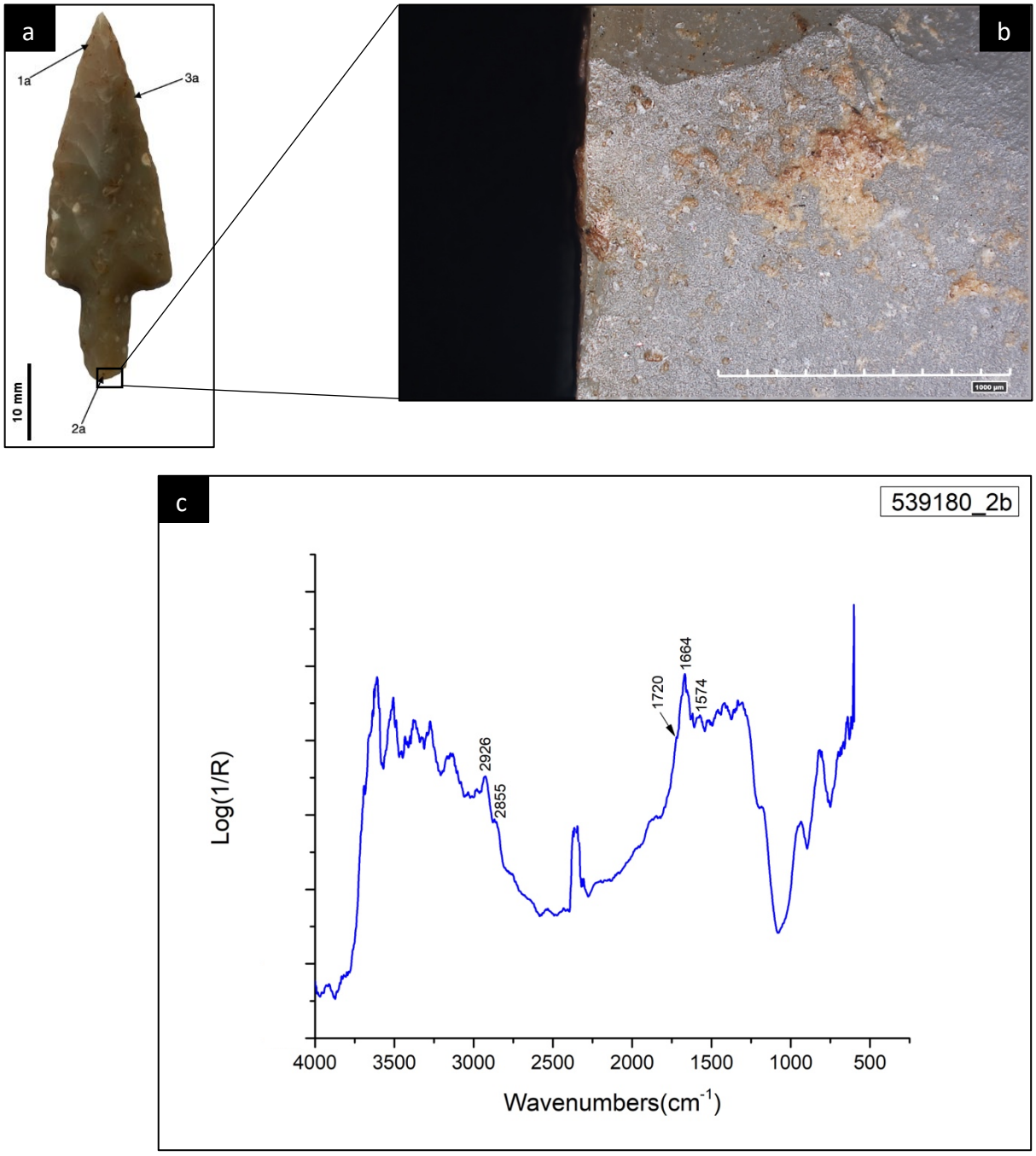


**Figure 35:** Tool number 539180 with residue results. (a) Tool number 539180 showing residue map. (b) Brown amorphous residues (RLM Micrograph, 1000µm). (c) micro-FTIR spectrum of the residue

4. Tool number 539181

The results of Tool number 539181 from Tomb 14 can be seen in Figure 43. The residues are located at the tip of the arrowhead (Fig. 32a) and consist of dark amorphous residues along with some fibre and sediments (Fig. 32b). The micro-FTIR results show peaks attributed to C-H stretching modes at 2922 and 2861 $cm^{-1}$ confirming the presence of organic materials in the sample.

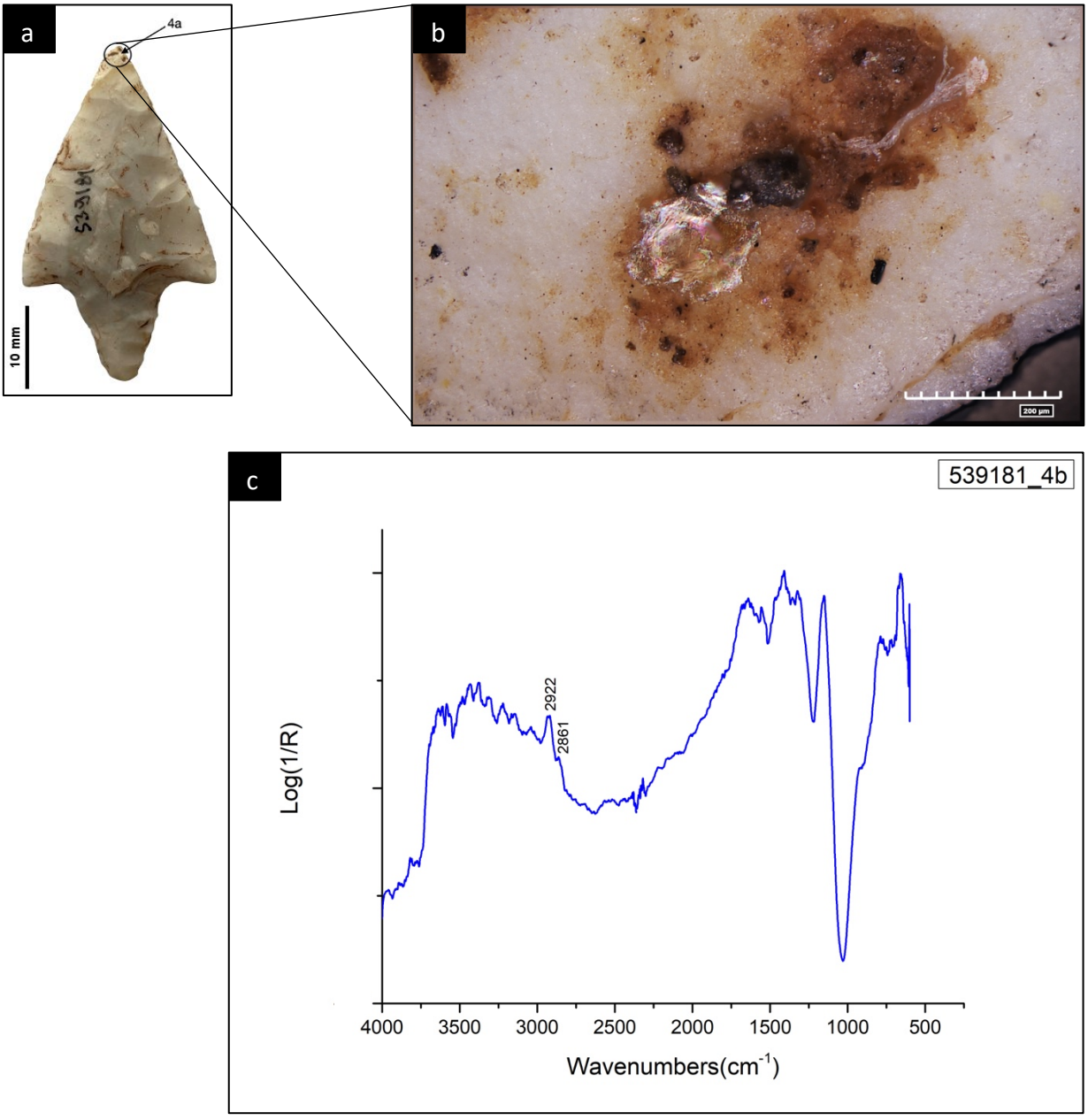


**Figure 36:** Tool number 539181 with residue results. (a) Tool number 539181 showing residue map. (b) Brown amorphous residues along with sediments (RLM Micrograph, 200µm). (c) micro-FTIR spectrum of the residue

## 4.2 Discussion

The objective of this research was to record every micro residue that was found on the stone tools, to characterise those residues using a variety of techniques, and to determine whether or not inorganic, and especially organic residues had been maintained on the stone tool surfaces throughout years of burial. The employed methodology involved several steps. Firstly, the stone tools were scanned using RLM to document the residues' location and overall appearance. Secondly, the tools were scanned under SEM to obtain EDS spectra and identify any additional residues. Thirdly, the residues were analysed using FTIR microscopy. This comprehensive approach allowed us to collect multiple lines of data for numerous residues, thereby confirming the presence of inorganic and organic residues. The work further demonstrates the feasibility of doing non-invasive in-situ examination of organic residues by employing the technique of Fourier Transform Infrared Microscopy (FTIR-M).

A total of 5 tools were recovered from Tomb 3. Out of those, 3 tools were analysed for residues, and only one (Figure 10) showed the presence of organic residues. The identification of distinct peaks associated with hydrocarbon and carbonyl groups provides evidence for the existence of organic materials on the surface of the stone tool.

A collective sum of 42 foliate points were unearthed from Tomb 4. A total of five samples were subjected to residue analysis, and among them, three samples showed indications of organic residues. All of them show peaks attributed to C–H stretching modes confirming the presence of organic residues. The presence of the shoulder at 1720 $cm^{-1}$(Figure 11) indicates the presence of fatty acids in the sample. The contents of Tomb 4 make it one of the richest tombs in the necropolis. It has been hypothesised that the individual was a male and between the ages of 20 and 30 years old, based on the characteristics of the burial goods (Anzidei & Carboni, 2020a). The presence of Cinnabar on the foliate points inside the tomb is probably ritualistic in nature and could be attributed to the importance of the individual buried considering its rare occurrence. Similar evidence of lumps of Cinnabar being sprinkled in graves can be found in other Chalcolithic sites from Italy also like Lucrezia Romana, Ponte delle sette Miglia, Lunghezzina, etc (Anzidei & Carboni, 2020a).

The findings of a study conducted on the use-wear traces on a sample of 12 foliate points from Tomb 4, showed evidence of usage on 5 of them (Lemorini, et al., 2020). The presence of long-lasting contact traces on the tang and shoulder area, as well as indications of direct polishing on the tip, suggests that this artefact was utilised as a projectile.

The contents of Tomb 5 yielded a total of 20 foliate points, out of which 18 were analysed for traces of residues. Out of these, 8 foliate points showed signs of organic material. proteinaceous materials were found on 5 of these foliate points with Tool No. 539207 (Figure 15), 539215 (Figure 19) and 539224 (Figure 23) also showing the presence of fat due to its attribution to the carbonyl group. The presence of proteinaceous material and fatty acids on the same sample could potentially indicate its use on animal material.

There was a total of 9 flint points unearthed from Tomb 7, and all of them were analysed for residues; out of the nine, three showed signs of having organic residues on them. The analysis revealed that just a single artefact (Figure 26 and 27) exhibited indications of the presence of proteinaceous material on the sample due to the presence of Amide I and II peaks. The remaining two artefacts exhibit distinctive C-H stretching modes, which are indicative of the occurrence of organic materials.

A comprehensive analysis was conducted on all seven flint points recovered from Tomb 14. Among the seven samples, four exhibited indications of the presence of organic material. Three out of the four artefacts exhibit peaks corresponding to Amide I and II, suggesting the existence of proteinaceous materials.

The data presented in this study demonstrates that it is possible to obtain reflectance Fourier-transform infrared Microspectroscopy (FTIR-M) spectra for archaeological remains that have undergone long-term burial. The quality of the spectrum is determined by the fundamental characteristics of the sample. The residues from Torre della Chiesaccia exhibit significant degradation and are extensively interspersed with sediments originating from the tomb. The challenge of obtaining high-quality reflectance spectra for the organic residues was attributed to this particular issue. This particular issue was tackled by obtaining multiple spectrums from the same spot. As shown in Figure 35, the same spot exhibits differences in their spectrum. The blue line (539178_1b_p2) is the one used in the study showing characteristic amide peaks; the red line (539178_1b) also exhibits amide peaks but it is weaker and not very prominent. A further contributing factor in addressing this particular issue was the reduction of the microscope's aperture size (Monnier, et al., 2018). This adjustment served to minimise the interference caused by the stone background.

An additional complicated element arose from the presence of reststrahlen bands (Monnier, et al., 2018) (Lemorini, et al., 2020) (Prinsloo, et al., 2014) (Solodenko, et al., 2015) (Zupancich, et al., 2016) within the range of 1300 to 1000 $cm^{-1}$, resulting in spectral distortion. As a consequence of this phenomenon, a considerable number of the spectra acquired exhibit

limited interpretability due to distortions arising from the extensive reststrahlen band generated by siliceous stone. Certain compounds have a distinct peak within this particular peak. In the context of bone samples, it is seen that the hydroxyapatite peak appears at around 1040 $cm^{-1}$, which regrettably remains undetectable on the spectra.

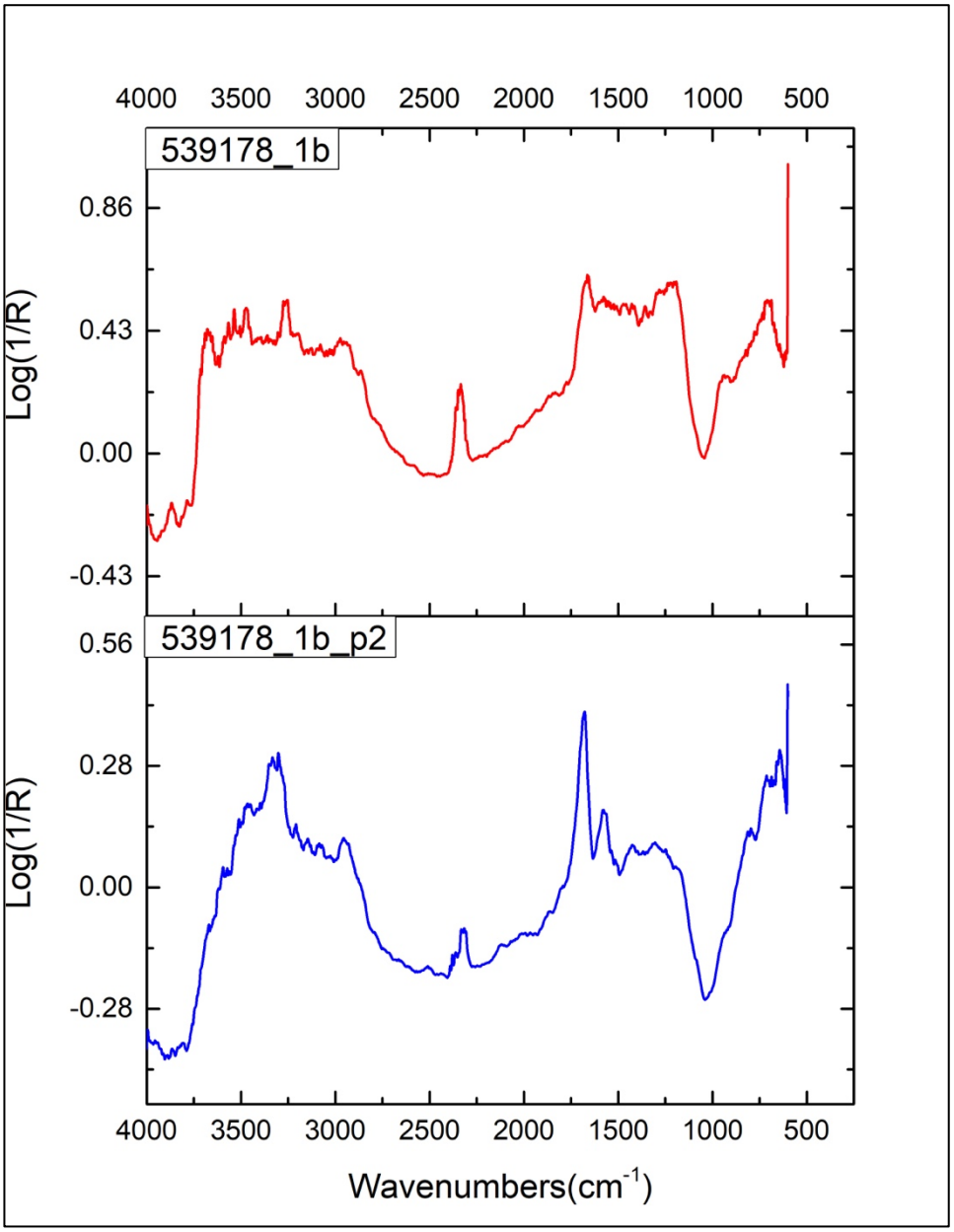


**Figure 37:** micro-FTIR spectrum of Residue No. 539178_1b showing differences in the Amide peaks

The residues present on artefacts exhibit heterogeneity and undergo modifications as a result of chemical diagenesis, leading to changes in their optical characteristics. The bone residue presented in Figure 29 of our study is an exceptional specimen, as the preservation of such residues is quite uncommon. As seen by the previously discussed samples, the residue is

predominantly observed in an amorphous state and does not consistently preserve its morphological attributes. The residues have undergone crushing, maceration, and subsequent diagenesis as a result of their dynamic life cycle, resulting in alterations to their morphological properties. Moreover, this implies that there is an expectation of observing variations in the composition of ancient residues, which align with diagenetic mechanisms like oxidation and hydrolysis. Many of the samples had a significant concentration of water, as seen by the presence of OH absorptions between 3000 and 3800 $cm^{-1}$. This observation can be attributed to the process of hydrolysis.

Previous studies have demonstrated that the identification of macerated, smeared, and extensively degraded residues, which are comparable to those often seen in archaeological contexts, poses challenges and calls for the use of supplementary analytical tools for accurate identification (Hayes & Rots, 2019). Hence, despite the limited preservation of certain morphological attributes of the residues, the application of supplementary chemical analysis techniques such as FTIR-M demonstrates their effectiveness in the identification of organic residues.

The findings of our research, tentative at present, indicate that tools obtained from burial contexts exhibit lasting use-residues, and the utilisation of several instruments can be a viable approach for identification and in-situ analysis. Since the artefacts belong to a Chalcolithic burial site, steps were taken to eliminate all possible modern contamination. As mentioned in Chapter 3, the artefacts were washed with neutral soap and water and residues with obvious contaminants like cloth fibre, graphite from pencil, etc were immediately discarded. On the basis of the location of the residues near the tip of the point and on the edges, and the fact that the residues were embedded in sediments on the tool, the presence of ancient contaminants can be provisionally eliminated for now. Future work combining the study of residues with use-wear analysis will allow for a more thorough functional analysis of the foliate points.

# 5. Conclusions

The data obtained from the study of use-residues from the Tombs 3, 4, 5, 7, and 14 from the cemetery of Torre della Chiesaccia show that the foliate points had a dynamic life cycle. On the basis of the results of the residue analysis and the use-wear (Lemorini, et al., 2020), it is evident that the flint points were used prior to their burial with the individual. However, it is possible that not all foliate points were daily objects of use and that some were just included as grave goods as not all the tools show evidence of use. This lack of evidence could also be attributed to a poor state of preservation of the use-residues.

This study shows that it is possible to detect organic residues on stone tool surfaces after prolonged burial. A total of 44 foliate points were analysed for this study, out of which 19 tools showed the presence of organic materials. A combination of multiple techniques has proven to be useful for the identification of use-residues. A study solely focusing on the morphology of the use-residues and its analysis with Reflected Light Microscopy was not feasible for a study of this kind as the morphological features of the residues have undergone severe degradation and therefore do not retain physical features. This makes it harder to identify the residues just on the basis of morphology. Therefore, use of FTIR-M as a complementary method for the in-situ analysis has proven to be successful. Future work combining use-wear and residue analysis will give a complete picture of the function of these flint points.

# 6. References


1. Anzidei, A. P. & Carboni, G., 2020a. ROMA PRIMA DEL MITO ABITATI E NECROPOLI DAL NEOLITICO ALLA PRIMA ETA' DEI METALLI NEL TERRITORIO DI ROMA (VI-III millennio a.C.) VOL 1. geologia, ambiente e fonti archeologiche. Oxford: Archaeopress Publishing Ltd.
2. Anzidei, A. P. & Carboni, G., 2020b. ROMA PRIMA DEL MITO ABITATI E NECROPOLI DAL NEOLITICO ALLA PRIMA ETA' DEI METALLI NEL TERRITORIO DI ROMA (VI-III millennio a.C.) VOL 2. aspetti culturali e contributi specialistici. Oxford: Archaeopress Publishing Ltd.
3. Anzidei, A. P. et al., 2008. Il Gaudo a Sud del Tevere: abitati e necropoli dall'area romana. Bologna, XLIII Riunione Scientifica - L'età del rame in Italia.
4. Barton, H., Torrence, R. & Fullagar, R., 1998. Clues to Stone Tool Function Re-examined: Comparing Starch Grain Frequencies on Used and Unused Obsidian Artefacts. Journal of Archaeological Science, Volume 25, pp. 1231-1238.
5. Berthomieu, C. & Hienerwadel, R., 2009. Fourier transform infrared (FTIR) spectroscopy. Photosynthesis Research, Issue 101, pp. 157-170.
6. Bhargava, R., Wang, S.-Q. & Koenig, J. L., 2003. FTIR Microspectroscopy of Polymeric Systems. Advances in Polymer Science, Issue 163, pp. 137-191.
7. Borel, A., Ollé, A., Vergès, J. M. & Sala, R., 2013. Scanning Electron and Optical Light Microscopy: two complementary approaches for the understanding and interpretation of usewear and residues on stone tools. Journal of Archaeological Science, pp. 1-14.
8. Briuer, F. L., 1976. New Clues to Stone Tool Function: Plant and Animal Residues. American Antiquity, 41(No 4), pp. 478-484.
9. Carboni, eds. ROMA PRIMA DEL MITO ABITATI E NECROPOLI DAL NEOLITICO ALLA PRIMA ETA' DEI METALLI NEL TERRITORIO DI ROMA (VI-III millennio a.C.) 2. aspetti culturali e contributi specialistici. Oxford: Archaeopress Publishing Ltd, pp. 429-436.
10. Carboni, G. et al., 2020. Le facies di Rinaldone e del Gaudo nel territorio di Roma: nuovi dati sulla circolazione di beni di prestigio e sulla mobilità di gruppi umani nell'ambito del bacino mediterraneo. Rivista di Scienze Preistoriche, Volume LXX S1, pp. 469-476.

11. Cârciumaru, M., Ion, R.-M., Niţu, E.-C. & Ștefănescu, R., 2012. New evidence of adhesive as hafting material on Middle and Upper Palaeolithic artefacts from Gura Cheii-Râsnov Cave (Romania). Journal of Archaeological Science, Volume 39, pp. 1942-1950.
12. Cnuts, D. & Rots, V., 2018. Extracting residues from stone tools for optical analysis: towards an experiment-based protocol. Archaeol Anthropol Sci, pp. 1717-1736.
13. Cnuts, D., Peresani, M. & Rots, V., 2022. The contribution of stone tool residues in reconstructing Late Pleistocene hominin stone tool behaviour at Grotta di Fumane, Italy. Quaternary Science Reviews, Volume 297.
14. Croft, S., 2021. Lithic Residue Analysis. Oxford: BAR Publishing.
15. Croft, S., Chatzipanagis, K., Kröger, R. & Milner, N., 2018. Misleading residues on lithics from Star Carr: Identification with Raman Microspectroscopy. Journal of Archaeological Science: Reports, Volume 19, pp. 430-438.
16. Dinnis, R., Pawlik, A. & Gaillard, C., 2009. Bladelet cores as weapon tips? Hafting residue identification and micro-wear analysis of three carinated burins from the late Aurignacian of Les Vachons, France. Journal of Archaeological Science, 36(9), pp. 1922-1934.
17. Frahm, E. et al., 2022. Every contact leaves a trace: Documenting contamination in lithic residue studies at the Middle Palaeolithic sites of Lusakert Cave 1 (Armenia) and Crvena Stijena (Montenegro). PLoS ONE, Volume 17.
18. Groman-Yaroslavski, I., Zaidner, Y. & Weinstein-Evron, M., 2021. Complexity and sophistication of Early Middle Palaeolithic flint tools revealed through use-wear analysis of tools from Misliya Cave, Mount Carmel, Israel. Journal of Human Evolution 154.
19. Guglielmi, V. et al., 2022. The combined use of SEM-EDX, Raman, ATR-FTIR and visible reflectance techniques for the characterisation of Roman wall painting pigments from Monte d'Oro area (Rome): an insight into red, yellow and pink shades. Environmental Science and Pollution Research, Volume 29, pp. 29419-29437.
20. Hardy, B. L. et al., 2013. Impossible Neanderthals? Making string, throwing projectiles and catching small game during Marine Isotope Stage 4 (Abri du Maras, France). Quaternary Science Reviews, Volume 82, pp. 23-40.
21. Hardy, B. L. et al., 2020. Direct evidence of Neanderthal fibre technology and its cognitive and behavioural implications. Scientific Reports, Volume 10, p. 4889.

22. Hayes, E. & Rots, V., 2019. Documenting scarce and fragmented residues on stone tools: an experimental approach using optical microscopy and SEM-EDS. Archaeological and Anthropological Sciences, Volume 11, pp. 3065-3099.
23. Hayes, E., Cnuts, D. & Rots, V., 2019. Integrating SEM-EDS in a sequential residue analysis protocol: Benefits and challenges. Journal of Archaeological Science: Reports 23, pp. 116-126.
24. Helwig, K., Monahan, V., Poulin, J. & Andrews, T. D., 2014. Ancient projectile weapons from ice patches in north-western Canada: identification of resin and compound resin-ochre hafting adhesives. Journal of Archaeological Science, Volume 41, pp. 655-665.
25. Lemorini, C. et al., 2020. The use of ash at Late Lower Palaeolithic Qesem Cave, Israel—An integrated study of use-wear and residue analysis. PLoS ONE, 15(9).
26. Lemorini, C. et al., 2022. Life Around the Elephant in Space and Time: An Integrated Approach to Study the Human Elephant Interactions at the Late Lower Palaeolithic Site of La Polledrara di Cecanibbio (Rome, Italy). Journal of Archaeological Method and Theory.
27. Lemorini, C., Caricola, I. & Cesaro, S. N., 2020. Le punte foliate dai contesti funerari di Torre della Chiesaccia (Roma): analisi delle tracce d'uso e dei residui. In: A. P. Anzedei & G.
28. Loy, T. & Lamb, J., 2005. Seeing red: the use of Congo Red dye to identify cooked and damaged starch grains in archaeological residues. Journal of Archaeological Science, 32(10), pp. 1433-1440.
29. Loy, T. H., 1983. Prehistoric Blood Residues: Detection on Tool Surfaces and Identification of Species of Origin. Science, 220(4603), pp. 1269-1271.
30. Monnier, G. & May, K., 2019. Documenting the degradation of animal-tissue residues on experimental stone tools: a multi-analytical approach. Archaeological and Anthropological Sciences, Issue 11, pp. 6803-6827.
31. Monnier, G. F. et al., 2013. A multi-analytical methodology of lithic residue analysis applied to Palaeolithic tools from Hummal, Syria. Journal of Archaeological Science 40, pp. 3722-3739.
32. Monnier, G. F., Ladwig, J. L. & Porter, S. T., 2012. Swept under the rug: the problem of unacknowledged ambiguity in lithic residue identification. Journal of Archaeological Science 39, pp. 3284-3300.

33. Monnier, G., Frahm, E., Luo, B. & Missal, K., 2017. Developing FTIR Microspectroscopy for analysis of plant residues on stone tools. Journal of Archaeological Science, Issue 78, pp. 158-178.
34. Monnier, G., Frahm, E., Luo, B. & Missal, K., 2018. Developing FTIR Microspectroscopy for the Analysis of Animal-Tissue Residues on Stone Tools. Journal of Archaeological Method and Theory, Issue 25, pp. 1-44.
35. Nelson, D. E., Loy, T. H., Vogel, J. S. & Southon, J. R., 1986. Radiocarbon dating blood residues on prehistoric stone tools. Radiocarbon, 28(No. 1), pp. 170-174.
36. Nucara, A., Nunziante-Cesaro, S., Vendetti, F. & Lemorini, C., 2020. A multivariate analysis for enhancing the interpretation of infrared spectra of plant residues on lithic artefacts. Journal of Archaeological Science: Reports, Issue 33.
37. Pawlik, A. F. & Thissen, J. P., 2011. Hafted armatures and multi-component tool design at the Micoquian site of Inden-Altdorf, Germany. Journal of Archaeological Science, Volume 38, pp. 1699-1708.
38. Pedergnana, A. & Blasco, R., 2016. Characterising the exploitation of avian resources: An experimental combination of lithic use-wear, residue and taphonomic analyses. Quaternary International, Volume 421, pp. 255-269.
39. Pedergnana, A. & Ollé, A., 2018. Building an Experimental Comparative Reference Collection for Lithic Micro-Residue Analysis Based on a Multi-Analytical Approach. Journal of Archaeological Method and Theory 25, pp. 117-154.
40. Pedergnana, A., 2020. “All that glitters is not gold”: Evaluating the Nature of the Relationship Between Archaeological Residues and Stone Tool Function. Journal of Paleolithic Archaeology, pp. 225-254.
41. Pedergnana, A., Asryan, L., Fernández-Marchena, J. & Ollé, A., 2016. Modern contaminants affecting microscopic residue analysis on stone tools: A word of caution. Micron, Volume 86, pp. 1-21.
42. Prinsloo, L. C., Wadley, L. & Lombard, M., 2014. Infrared reflectance spectroscopy as an analytical technique for the study of residues on stone tools: potential and challenges. Journal of Archaeological Science, Issue 41, pp. 732-739.
43. Rots, V. et al., 2016. Making Sense of Residues on Flaked Stone Artefacts: Learning from Blind Tests. PLoS ONE.

44. Solodenko, N. et al., 2015. Fat Residue and Use-Wear Found on Acheulian Biface and Scraper Associated with Butchered Elephant Remains at the Site of Revadim, Israel. PLoS ONE, Issue 10.
45. Tomasso, S., Cnuts, D., Mikdad, A. & Rots, V., 2020. Changes in hafting practices during the Middle Stone Age at Ifri n' Ammar. Quaternary International, Volume 555, pp. 21-32.
46. Vendetti, F. et al., 2019. Animal residues found on tiny Lower Palaeolithic tools reveal their use in butchery. Scientific Reports, Volume 9.
47. Zupancich, A. et al., 2016. Early evidence of stone tool use in bone working activities at Qesem Cave, Israel. Scientific Reports, Issue 6, p. 37686.

# 7. Supplementary data

| Tomb Number | Tool Number | Residue Number | EDX data (In ascending order) | FTIR-M peak | Proposed assignment |
|---|---|---|---|---|---|
| Tomb 3 | 539108 | 539108_7b | × | 2916 $cm^{-1}$ | C–H stretching |
| | | | | 1720 $cm^{-1}$ | C = O stretching |
| Tomb 4 | 539134 | 539134_1a | × | 2936 $cm^{-1}$ | C–H stretching |
| | | | | 2860 $cm^{-1}$ | C–H stretching |
| | | | | 1720 $cm^{-1}$ | C = O stretching |
| | | | | 1537 $cm^{-1}$ | $CH_x$ bending |
| | | 539134_5b | × | 2947 $cm^{-1}$ | C–H stretching |
| | | 539134_6a | × | 2935 $cm^{-1}$ | C–H stretching |
| | | | | 2867 $cm^{-1}$ | C–H stretching |
| Tomb 4 | 539157 | 539157_2a | Hg, Ti, O, Fe, C, Al | × | × |
| Tomb 5 | 539207 | 539207_5b | × | 3290 $cm^{-1}$ | Amide A |
| | | | | 3082 $cm^{-1}$ | Amide B |
| | | | | 2930 $cm^{-1}$ | C–H stretching |
| | | | | 2859 $cm^{-1}$ | C–H stretching |
| | | | | 1715 $cm^{-1}$ | C = O stretching |
| | | | | 1653 $cm^{-1}$ | Amide I |
| | | | | 1593 $cm^{-1}$ | Amide II |
| | | 539207_8a | × | 2929 $cm^{-1}$ | C–H stretching |
| | | | | 2875 $cm^{-1}$ | C–H stretching |
| | | | | 1624 $cm^{-1}$ | Amide I |
| | | | | 1581 $cm^{-1}$ | Amide II |
| | | | | 1248 $cm^{-1}$ | Amide III |
| Tomb 5 | 539208 | 538208_3a | × | 3467 $cm^{-1}$ | Amide A |
| | | | | 3046 $cm^{-1}$ | Amide B |
| | | | | 1639 $cm^{-1}$ | Amide I |
| | | | | 1584 $cm^{-1}$ | Amide II |
| Tomb 5 | 539210 | 539210_3a | × | 2931 $cm^{-1}$ | C–H stretching |

| | | | | | |
|---|---|---|---|---|---|
| | | | | 2862 $cm^{-1}$ | C–H stretching |
| | | | | 1676 $cm^{-1}$ | Amide I |
| | | | | 1584 $cm^{-1}$ | Amide II |
| Tomb 5 | 539215 | 539215_2a | × | 2950 $cm^{-1}$ | C–H stretching |
| | | | | 2852 $cm^{-1}$ | C–H stretching |
| | | | | 1722 $cm^{-1}$ | C = O stretching |
| | | | | 1668 $cm^{-1}$ | Amide I |
| | | | | 1543 $cm^{-1}$ | Amide II |
| | | | | 1441 $cm^{-1}$ | $CH_x$ bending |
| Tomb 5 | 539220 | 539220_3a | × | 2924 $cm^{-1}$ | C–H stretching |
| | | | | 2859 $cm^{-1}$ | C–H stretching |
| | | | | 1630 $cm^{-1}$ | Amide I |
| | | | | 1544 $cm^{-1}$ | Amide II |
| Tomb 5 | 539222 | 539222_3a | × | 2928 $cm^{-1}$ | C–H stretching |
| | | | | 2865 $cm^{-1}$ | C–H stretching |
| Tomb 5 | 539223 | 539223_4a | × | 2940 $cm^{-1}$ | C–H stretching |
| | | | | 2865 $cm^{-1}$ | C–H stretching |
| Tomb 5 | 539224 | 539224_1a | × | 2931 $cm^{-1}$ | C–H stretching |
| | | | | 2861 $cm^{-1}$ | C–H stretching |
| | | | | 1721 $cm^{-1}$ | C = O stretching |
| | | | | 1454 $cm^{-1}$ | $CH_x$ bending |
| Tomb 7 | 539190 | 539190_1b | × | 2936 $cm^{-1}$ | C–H stretching |
| | | | | 2860 $cm^{-1}$ | C–H stretching |
| | | 539190_6a | × | 2941 $cm^{-1}$ | C–H stretching |
| | | | | 2859 $cm^{-1}$ | C–H stretching |
| Tomb 7 | 539192 | 539192_4a | O, Si, Br, C, Na | 2931 $cm^{-1}$ | C–H stretching |
| | | | | 2861 $cm^{-1}$ | C–H stretching |
| | | | | 1635 $cm^{-1}$ | Amide I |

| | | | | | |
|---|---|---|---|---|---|
| | | | | 1588 $cm^{-1}$ | Amide II |
| | | 539192_10a | × | 2927 $cm^{-1}$ | C–H stretching |
| | | | | 2868 $cm^{-1}$ | C–H stretching |
| | | | | 1628 $cm^{-1}$ | Amide I |
| | | | | 1580 $cm^{-1}$ | Amide II |
| Tomb 7 | 539195 | 539195_1a | × | 2926 $cm^{-1}$ | C–H stretching |
| | | | | 2855 $cm^{-1}$ | C–H stretching |
| Tomb 14 | 539178 | 539178_1b | Ca, P, Fe, O, W, F, Si, Al, C, S | 2961 $cm^{-1}$ | C–H stretching |
| | | | | 1679 $cm^{-1}$ | Amide I |
| | | | | 1578 $cm^{-1}$ | Amide II |
| | | 539178_3b | × | 2930 $cm^{-1}$ | C–H stretching |
| | | | | 2863 $cm^{-1}$ | C–H stretching |
| | | | | 1653 $cm^{-1}$ | Amide I |
| | | | | 1589 $cm^{-1}$ | Amide II |
| Tomb 14 | 539179 | 539179_3a | × | 2934 $cm^{-1}$ | C–H stretching |
| | | | | 2874 $cm^{-1}$ | C–H stretching |
| | | | | 1720 $cm^{-1}$ | C = O stretching |
| | | | | 1641 $cm^{-1}$ | Amide I |
| | | | | 1535 $cm^{-1}$ | Amide II |
| | | 539179_12a | × | 2943 $cm^{-1}$ | C–H stretching |
| | | | | 2868 $cm^{-1}$ | C–H stretching |
| | | | | 1655 $cm^{-1}$ | Amide I |
| | | | | 1535 $cm^{-1}$ | Amide II |
| Tomb 14 | 539180 | 539180_2b | × | 2926 $cm^{-1}$ | C–H stretching |
| | | | | 2855 $cm^{-1}$ | C–H stretching |
| | | | | 1720 $cm^{-1}$ | C = O stretching |
| | | | | 1664 $cm^{-1}$ | Amide I |
| | | | | 1574 $cm^{-1}$ | Amide II |
| Tomb 14 | 539181 | 539181_4b | × | 2922 $cm^{-1}$ | C–H stretching |
| | | | | 2861 $cm^{-1}$ | C–H stretching |